Research Article

Numerical study on hybrid metallic sandwich structures subjected to air burst

Solomon Abebe Derseh[1] · Tesfaye Alemu Mohammed[2] · Girum Urgessa[3]

© The Author(s) 2023   OPEN

Abstract

This study presents a numerical investigation on the use of previously unexplored hybrid sandwich protective structural configurations with aim to resist airblast loading. A honeycomb, corrugated sheet, and woven interlaced core configurations are used to develop the hybrid system. An experimental result reported in the previous literature is used for validation of the finite element analysis models using Abaqus/Explicit finite element software with a conventional weapon blast related parametric codes. Then an extended numerical study is conducted further on various hybrid sandwich inner core topologies for maximizing protection against an air blast induced shock wave. The study demonstrated that a protective system, combining square honeycomb metallic cores with X-shaped corrugated sheets and fortified against in-plane compression and buckling, showed excellent shielding capabilities against airblast loading. This configuration also exhibited the highest energy dissipation, the least effective plastic strain, minimal back sheet displacement, and a favorable damage profile.

Article highlights

- The paper proposes a new hybrid sandwich protective structure to resist blast loading.
- A new hybrid sandwich protective panel construction is also introduced.
- Among the various panels studied, the hybrid panel that utilized both honeycomb and cross-shaped cores demonstrated effective blast shielding capability.

1 Introduction

Blast loading poses risks to lives and structures. Metallic sandwich panels, incorporating honeycomb, corrugated, and woven cellular cores, demonstrate potential for damage mitigation through plastic deformation. However, further research is required to assess the energy dissipation capabilities of these hybrid structures against airblast loading. In sandwich structures, the inner cellular cores play an important role in protecting a given asset and serve as a shield against abnormal loads such as impact, blast and synergetic effects of combined blast-impact loads [1]. In addition to this, according to [2], in order to mitigate the damage induced by abnormal

✉ Solomon Abebe Derseh, solomon_abebe@dmu.edu.et | [1]Department of Civil Engineering, Debre Markos University, Debre Markos, Ethiopia. [2]Department of Civil Engineering, Addis Ababa Science and Technology University, Addis Ababa, Ethiopia. [3]Department of Civil, Environmental, and Infrastructure Engineering, George Mason University, Fairfax, USA.

loads, the main technology recommendations on which the sandwich structures shall be designed are continuity of structures, reserve strength in excess of live loads, redundancy in load bearing paths and increased energy absorptions.

Metallic sandwich panels can be divided into different types such as honeycomb, lattice truss, folded, woven, auxetic, and tubular cores [3, 4]. Consequently, whenever a sandwich panel is composed of those cellular cores namely honeycomb, lattice truss, folded, woven interlace etc., it is termed as hybrid sandwich protective structure.

Existing research in this field primarily examines the performance of various sandwich structures under blast loading. Some studies focus on stainless-steel alloy with honeycomb cores [3–8], while others investigate corrugated sheets embedded in sandwich panels under different compression loads [2, 9–12]. Additionally, there are works on auxetic sandwich structures to withstand blast-induced shock waves [8, 13, 14]. Both connected and unconnected layer connection systems are recommended for constructing protective panels [1–3], and 3D printed cellular metallic cores with monolithic facet panels have also been explored [13, 14].

However, detailed quantification of damage response and effectiveness of sandwich panels comprised by hybrid cellular metallic cores with numerous unforeseen structural configurations to resist an air burst is limited. Thus, the present study employed Abaqus/Explicit finite element analysis (FEA) to develop the spatial 3D FEA models considering both the geometrical and material nonlinear properties. The airblast loading simulation was performed using conventional weapon (ConWep) code. The back sheet nodal displacement, damage and energy dissipation response of the FEA models were evaluated in terms of an extracted effective plastic strain, viscous, artificial, plastic, total energy and displacement–time history plots. The innovation of the present study is that, all the proposed novel hybrid systems were designed by simultaneous use of a honeycomb, corrugated sheet, and woven interlaced core configurations.

In the present study, section one is all about the introduction about numerical investigation of hybrid metallic structures subjected to air burst. Section two deals with the finite element analysis accompanied by detailed description of the numerical model, element, material, and damage models, data acquisition procedures, loading, boundary conditions, and dynamic analysis steps. Moreover, the validation for the finite element model is also presented. Section three presents the parametric analysis results and discussions. It begins with describing the proposed parameters following with variation in back sheet nodal displacement, field stress and various energy values. In addition to this, the damage model of the finite element

models are all presented. In section four, the conclusion of the analyzed and discussed sections are all made.

2 Finite element analysis

In this study a three-dimensional model of a metallic sandwich panel with different hybrid cellular core configurations were developed.

2.1 Description of numerical model

The experimental study conducted by [4] was used for finite element analysis model validation. Figure 1 depicts schematic plot of experimentally reported metallic alloy sandwich panel with square cellular metal core. [4] Employed a honeycomb sandwich with a 610 mm×610 mm planar area accompanied by 5 mm thick two cover solid plates and 51 mm high cellular metal core with 0.76 mm thickness laid on by 30.5 mm spacing. An air burst type with 3 kg charge mass and 100 mm stand-off distance was imposed on the panel and distinguished panel displacement, panel indentation profile, and core crushing damage profiles were evaluated.

Taking advantage of symmetry, only one-quarter of the model with 305 mm×305 mm planar area accompanied by 5 mm thick two cover solid plates and 51 mm high cellular metal core with 0.76 mm thickness laid on by 30.5 mm spacing of the panel was modeled. The following sections present numerical modelling techniques and procedures employed in development of the models.

2.2 Element and material models

A reduced integration eight-node 3D solid homogenous hexagonal brick element was used to model both end plates. On the other hand, a reduced integration linear
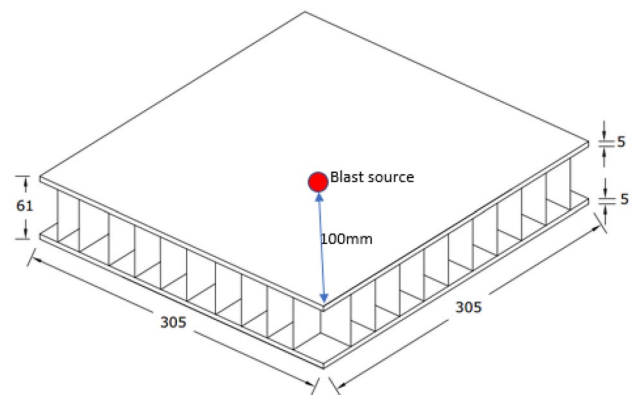

Fig. 1 Square honeycomb core sandwich panel for airblast test [4]

quadrilateral element with a four-node shell accompanied by 5 Simpson thickness integration points were employed to model cellular metallic cores. The Johnson–Cook material model, which includes analytical forms of hardening law, thermal and strain rate dependence was used as it is suitable for impulsive loads [4]. The flow yield stress in the Johnson–Cook material model is given by Eq. 1 [15, 16]:

$$\sigma_y = \left[A + B\left(\varepsilon_e^{pl}\right)^n \right] \left[1 + C \ln\left(\frac{\varepsilon_0'^{pl}}{\varepsilon_0'}\right) \right] \left(1 - \theta^m\right) \qquad (1)$$

where ε_0' is a reference strain rate, $c\varepsilon_e^{pl}$ is equivalent plastic strain, $\varepsilon_e'^{pl}$ is equivalent plastic strain rate, A, B, C, n, m are experimentally derived material constants, and in general the first bracket depicts the strain rate effect on the yield strength of the material and the second bracket terms accounts a thermal softening effect on the yield strength of the material. As shown in Eq. 2, θ is a normalized temperature defined in terms of absolute, melting, and transition temperature [15, 16].

$$\theta = \frac{T - T_{tr}}{T_M - T_{tr}} \qquad (2)$$

where, T, T_M, T_{tr} is an absolute, melting temperature and transition temperature, respectively.

2.3 Damage model

Damage in the Johnson–Cook material model was incorporated in the Johnson–Cook plasticity model accompanied by a value of equivalent plastic strain at element integration points which then further enables the material damage model to capture the gradual reduction in the load carrying capacity of a material. These values extracted from equivalent plastic strain at element integration points are sufficient to capture the gradual decrease in the load carrying capacity of a material leading to a total loss of strength. Abaqus initiates the creation of cracks during the simulation by searching for regions that are experiencing principal stresses and/or strains greater than the maximum damage values specified by the traction–separation laws [16]. Equation 3 lists a Johnson–Cook damage model (D) as a function of equivalent plastic and increment and failure states [17].

$$D = \sum \left(\frac{\Delta \varepsilon'}{\varepsilon_f'}\right) \qquad (3)$$

where $\Delta \varepsilon'$ is an equivalent plastic strain updated at every time increment and ε_f' shown in Eq. 4 is an equivalent

strain at failure state which can be expressed as follows [16, 17]

$$\varepsilon_f' = \left[D_1 + D_2 \exp\left(D_3 \frac{P}{\sigma'}\right) \right] \left[1 + D_4 \ln\left(\frac{\varepsilon'}{\varepsilon_0'}\right) \right] \left[1 + D_5 \left(\frac{T - T_{tr}}{T_M - T_{tr}}\right) \right] \qquad (4)$$

According to [17], failure in this model is perceived to occur when the damage parameters (D) listed in Table 1 are exceeded a value of unity. In the previous literature, [4, 15, 17] verified that the following Johnson Cook's constitutive and damage material models captured the dynamic properties of a honeycomb sandwich panel loaded with TNT explosives. Thus, the Johnson Cook constitutive material model and damage parameters employed in the present study are consistent with [4, 15, and 17] and are listed in Table 1.

2.4 Data acquisition, interaction and boundary condition

The top cover plate and back sheet displacement history of a finite element model along the distance of a cover plate was extracted by using Abaqus's nodal and path displacement extraction method. Two paths from the front and back cover plate faces were assigned as a source of data for displacement versus distance of the cover plate history curves. Furthermore, for nodal displacement–time history curve plots, a back sheet cover plate SET_NODE point, positioned directly beneath the TNT explosive charge mass, was assigned and traced (see Fig. 2).

The top and bottom side of honeycomb core were connected to top and bottom faces of a plate by using

Table 1 Johnson Cook's constitutive and damage material model input values for both the hybrid sandwich panel [17]

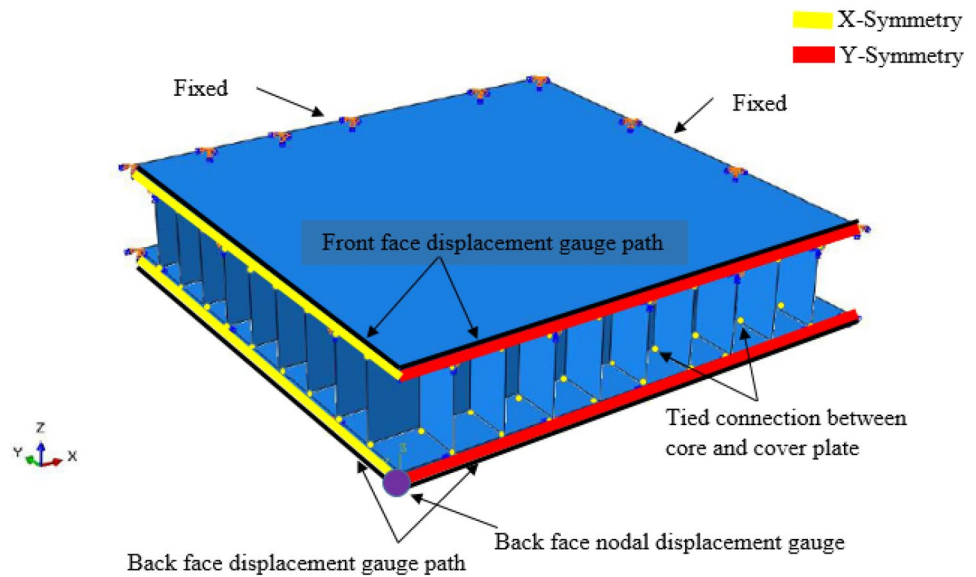| Parameter	Description	Unit	Values
E	Elastic modulus	GPa	161
υ	Poison ratio	–	0.35
ρ	Density	Kg/m^3	7850
ε_0'	Strain rate factor	s^{-1}	0.001
T_{tr}	Transition temperature	°C	20
T_M	Melting temperature	°C	1527
A	–	MPa	400
B	–	MPa	1500
C	–	–	0.045
n	–	–	0.4
m	–	–	1.2
D_1	Initial failure strain	–	−0.77
D_2	Exponential factor	–	1.45
D_3	Triaxiality factor	–	−0.47
D_4	Strain rate factor	–	0.0
D_5	Temperature factor	–	1.6

Fig. 2 Path, tied constraint, and boundary condition schemes of a honeycomb panel

the Abaqus/Explicit tie constrained command. After making sure that the face of the cellular cores were adjusted at their initial surface and tie rotational degree of freedom whenever applicable, the plate and cellular cores were assigned as master and slave nodes respectively. This constraint then ensures interface between cellular core and plate remains welded preventing relative displacement between respective interfaces. On the other hand, the interaction between the location of the explosive material and loaded face of the plate was assigned as a source and master surface respectively.

While doing so, the FEA model was developed by taking advantage of symmetry and only quarter of the sandwich structure with cellular metal core was modelled. Thus, symmetric boundary conditions on X and Y axis were applied at respective symmetric planes in X and Y axis on which the X-symmetry boundary condition restraints the translational degree of freedom at X-axis and rotational degree of freedoms at Y-and Z-axes. Likewise, the Y-symmetry boundary condition restraints the translational degree of freedom at Y-axis and rotational degree of freedoms at X-and Z-axes [16]. Moreover, since the referenced model was clamped against both translation and rotation, end sides of the finite element analysis model were fixed against translation and rotation by using a fixed restraint system on which both translational and rotational degree of freedoms about X, Y, and Z axes are all fixed (see also Fig. 2).

2.5 Blast loading and time steps

Air burst pressure was imposed on front face of a plate in accordance with ConWep code Eq. 5 shows the pressure that acts on front face of plate [4].

$$P = P_i \left[1 - \frac{t - t_a}{t_p} \right]^{-\frac{(t - t_a)}{\theta}} \tag{5}$$

where, P is total pressure on front face of a plate, P_i is incident pressure, t_a is arrival time, t_p is positive phase duration, t is total time duration, θ is exponential decay factor for incident wave.

A 3 kg explosive charge mass with 100 mm standoff distance from the center of the experimental reference model or edge nodal point of the FEA model was studied. A dynamic explicit type of step was deployed with a detonation and total analysis time of 0 and 1.5 ms respectively. The time increments were set to be in Abaqus/Explicit default setting and since the analysis was initiated by first activating the Nlgeom and global stable increment estimator module, it was fully a nonlinear-dynamic analysis.

2.6 Equivalent plastic strain and energy formulations

As stated in [16], the equivalent plastic strain (PEEQ) is a scalar variable utilized to represent a material's inelastic deformation. When PEEQ exceeds zero, it indicates material yielding. In ABQUS/Explicit, PEEQ is employed to formulate damage indices, as mentioned in Eq. 3.

Energy output is often an important part of an Abaqus/Explicit analysis. Energy balance (E_{total}) for the entire model is shown in Eq. 6. [16]:

$$E_I + E_V + E_{FD} + E_{KE} - E_W - E_{PW} - E_{CW} - E_{MW} = E_{total} = \text{Constant} \tag{6}$$

where E_I is the internal energy, E_V is the viscous dissipation on which it is the energy contribution to the total energy made by irreversible deformational work per unit time and volume, E_{FD} is the frictional energy dissipation, E_{KE} is the kinetic energy, E_W is the work done by the externally applied loads, and E_{PW}, E_{CW}, and E_{MW} are the work done by contact penalties, by constraint penalties, and by propelling added mass, respectively.

2.7 Finite element analysis model validation

Figure 3 illustrates a comparison between the experimental results [4] and the FEA numerical model for displacement values of the top (front) and bottom (back sheet) of the cover plate versus distance from the center of the plate. The maximum nodal displacement for the FEA was 150 mm and showed good agreement with experimental result and this mesh density was used for extended finite element analysis.
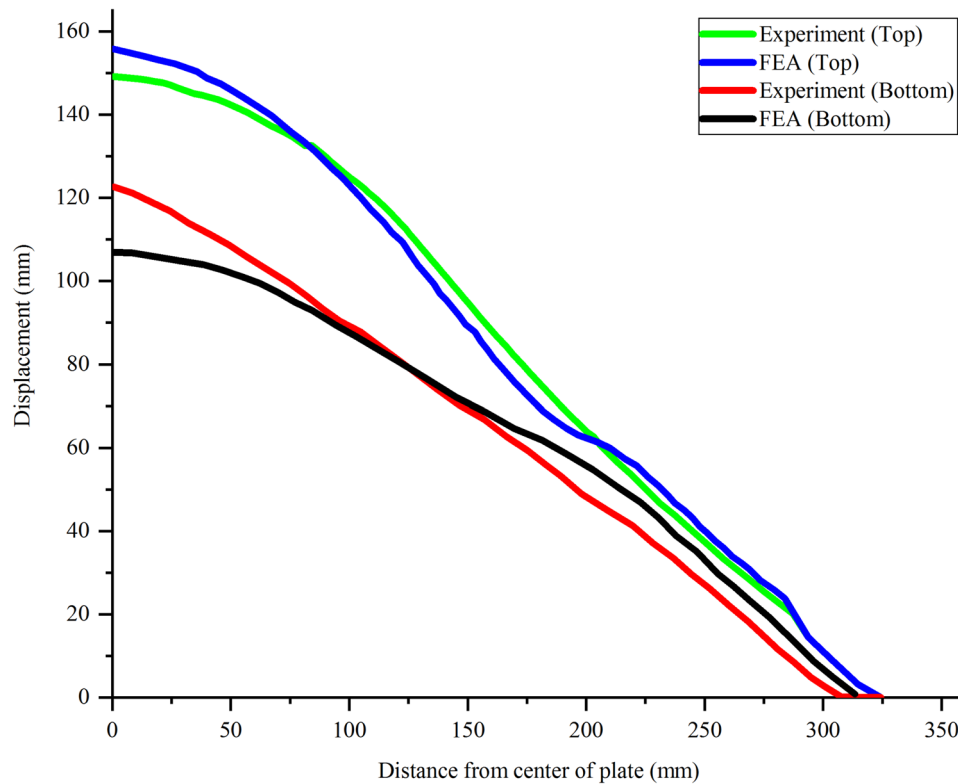
Fig. 3 Comparisons of top and bottom cover plate displacement versus distance from center of a plate
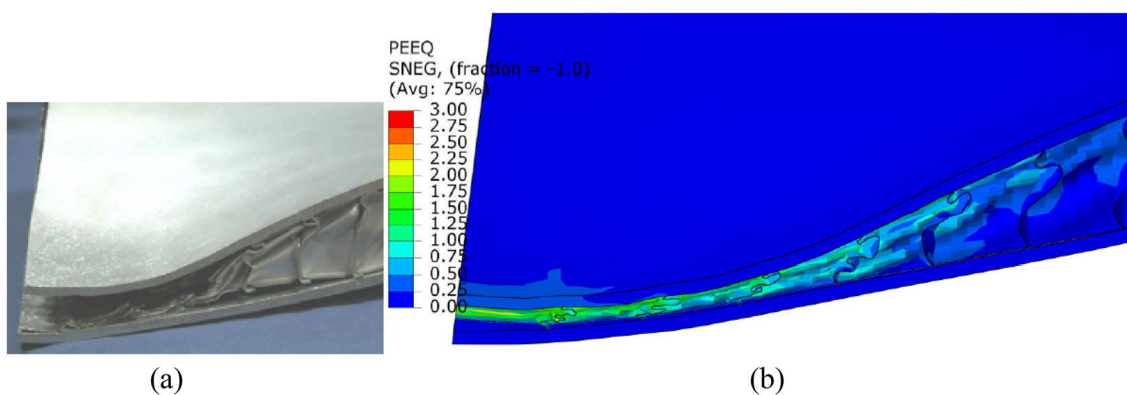
Fig. 4 Damage profile of a square honeycomb structure: (**a**) Experiment [4]; and (**b**) FEA

Moreover, both the experimental and FEA model showed good agreement in terms of high densification and indentation damage profile of the sandwich structure (Fig. 4). Moreover, as it is evident on both the experimental and FEA model results, a promising and visible cell wall buckling failure was predominantly observed on the exact location beneath the explosive. Besides this, going further away from the location of the detonation point, the core cells exhibited negligible buckling and folding. It can be confirmed that the FEA model captured the progressive transition from elastic to plastic buckling and folding of cellular metallic core walls.

3 Parametric study analysis, result and discussions

3.1 Description of parameters

The validated square shaped honeycomb sandwich structure (SHC) with a 305 mm × 305 mm planar area

accompanied by 5 mm thick two cover solid plates and 51 mm high cellular metal core with 0.76 mm thickness laid on by 30.5 mm spacing of the panel was used to serve as a control model for the extended parametric study. Figure 5 shows the geometrical dimensions and 3D FEA model for SHC.

By taking the validated sandwich panel with square honeycomb cores (SHC) as a control model, additional eight novel sandwich panels with hybrid core configurations were proposed and evaluated under air burst type of blast scenario. The proposed eight novel hybrid sandwich panel configurations include honeycomb, corrugated sheet, and woven interlaced cores. Figure 6 and Table 2 exhibits the cross-sectional dimensions and 3D FEA parts and assembled panels of the proposed new hybrid core configurations.

The proposed panels consist of a 0.76 mm cellular wall thickness enclosed by top and bottom cover plates (each 5 mm thick). To ensure proper contact between the hybrid core configurations, a 1 mm inserted plate was
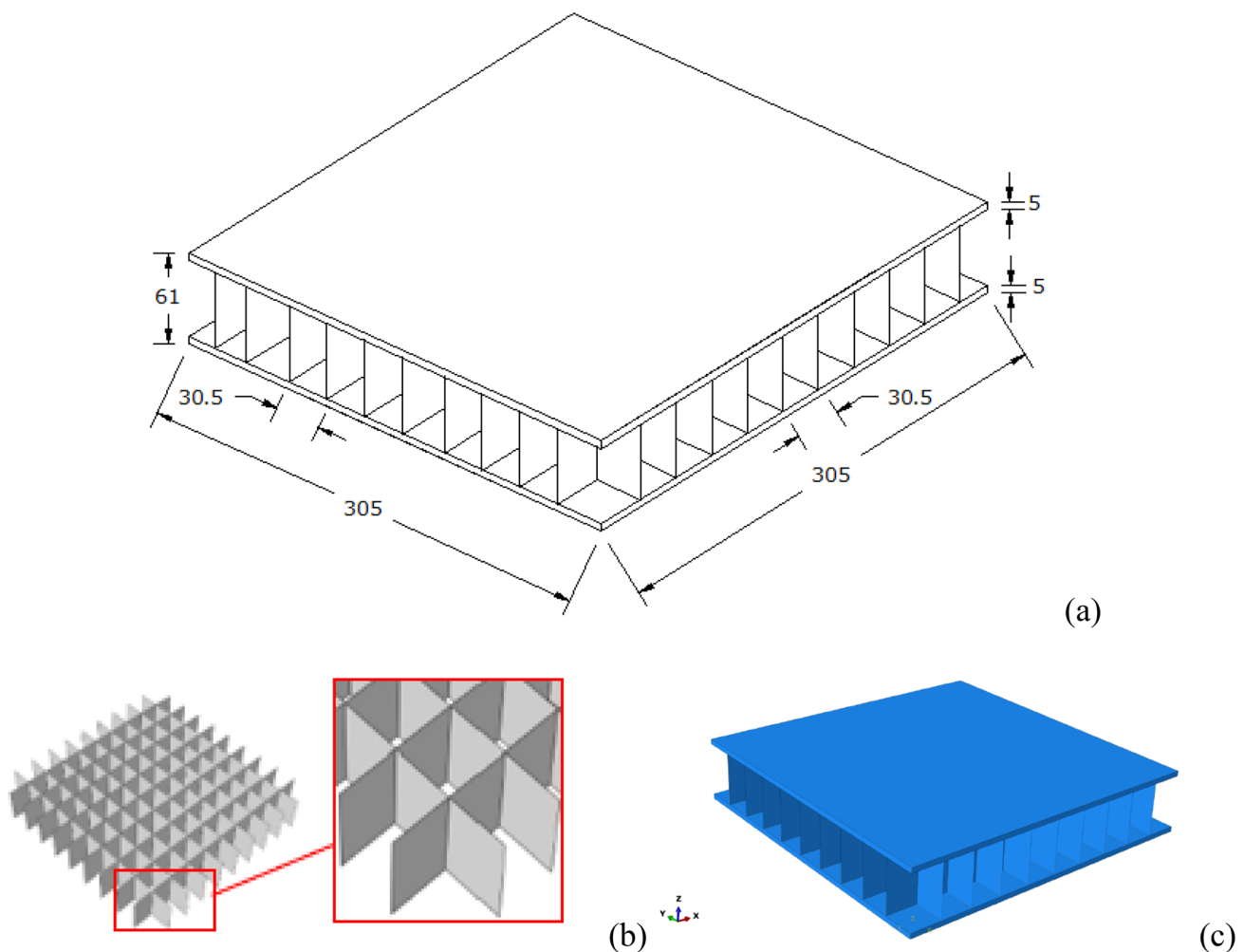
Fig. 5 Square honeycomb sandwich structure: (**a**) Geometrical dimension; (**b**) FEA cellular core part; and (**c**) Assembled 3D FEA model
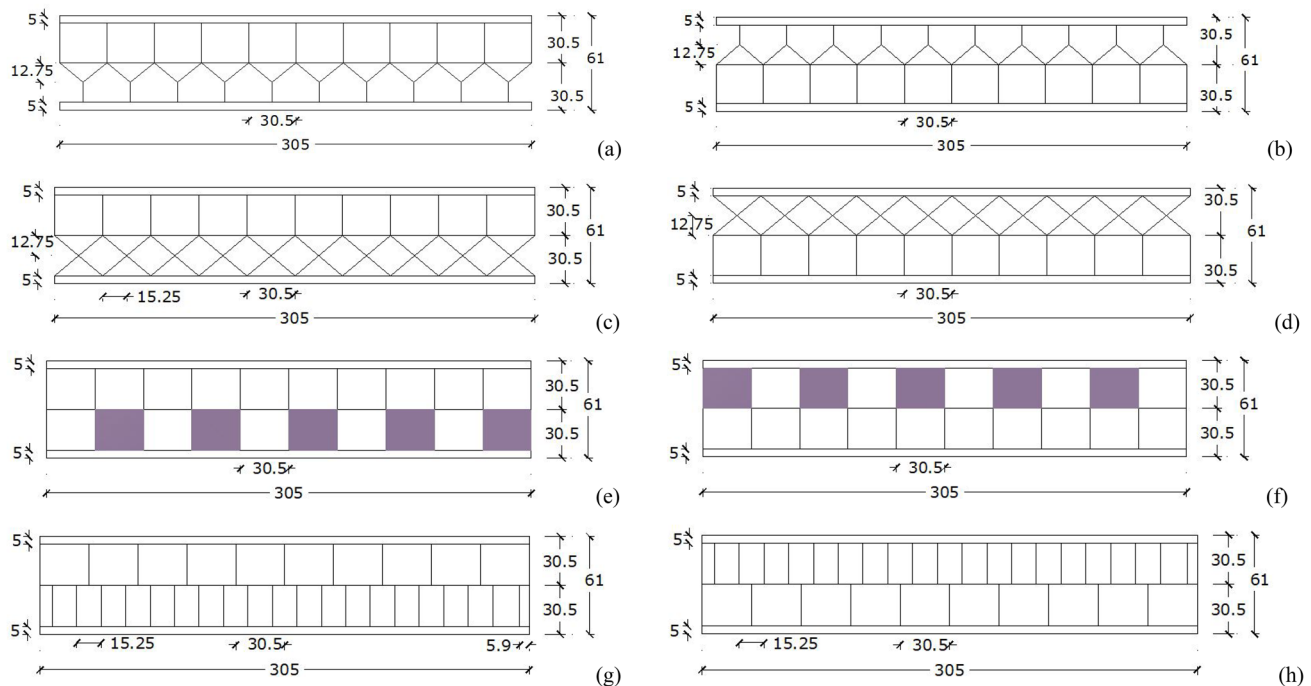
Fig. 6 Cross-sectional dimensions of the proposed hybrid metallic sandwich panels: (**a**); SHC_CYC; (**b**); CYC_SHC; (**c**); SHC_CXC; (**d**); CXC_SHC; (**e**); SHC_WSC; (**f**) WSC_SHC; (**g**); SHC_WTC; (**h**) WTC_SHC

placed between the top and bottom cores, facilitating layer contact in all the sandwich panels. This construction aligns with the connected type of sandwich construction described in [1–3, 13, 14]. The metallic cellular cores, inserted plate, and cover plates were tied together, effectively welded to prevent relative degrees of freedom.

From the proposed hybrid sandwich panel core configurations, the first one was a SHC_CYC configuration, where the panel had a top square shaped honeycomb core accompanied by a corrugated Y-shaped metallic sheets at the bottom (Fig. 6a and Table 2). A CYC_SHC on the other hand represented a hybrid sandwich structure with a corrugated Y-shaped metallic sheet at the top comprised by a square honeycomb core at the bottom (see Fig. 6b and Table 2).

The third proposed hybrid core configuration was a SHC_CXC configuration, where the panel had a square shaped honeycomb core located at the top accompanied by a corrugated X-shaped metallic sheets at the bottom (Fig. 6c and Table 2). A CXC_SHC on the other hand represented the fourth model with a corrugated X-shaped metallic sheet at the top comprised by a square honeycomb core at the bottom (see also Fig. 6d and Table 2).

The fifth hybrid core configuration was a SHC_WSC configuration, where the panel had a top square shaped honeycomb core accompanied by a sliced, woven square shaped metallic sheets at the bottom interlaced and oriented orthogonal to each other (Fig. 6e and Table 2). A

WSC_SHC on the other hand represented the sixth model with a sliced and woven square shaped metallic sheets at the top interlaced and oriented orthogonal to each other accompanied by a square honeycomb core at the bottom (see Fig. 6f and Table 2).

The seventh proposed hybrid core configuration was a SHC_WTC configuration, where the panel had a top square shaped honeycomb core accompanied by a sliced and woven triangular shaped metallic sheets at the bottom interlaced and oriented orthogonal to each other (Fig. 6g and Table 2). A WTC_SHC on the other hand represented the last eighth hybrid sandwich structure with a sliced and woven triangular shaped metallic sheets at the top interlaced and oriented orthogonal to each other accompanied by a square honeycomb core at the bottom (see also Fig. 6h and Table 2).

Three charge masses, 1 kg, 2 kg, and 3 kg trinitrotoluene (TNT) explosives located at 100 mm from the free end-node of the structures were considered. Moreover, with the validated sandwich structure with only honey comb core (SHC) was deployed as a control model and shielding capability of the other proposed novel hybrid sandwich panels were assessed based on the percentage difference in equivalent plastic strain, and energy-time histories of both SHC and hybrid sandwich structures.

Variation in peak equivalent plastic strain (PEEQ) values and viscous dissipation energy percentage differences of a sandwich structure with different hybrid core

Table 2 List of proposed hybrid metallic sandwich panel core configurations

Designation	Top core part	Bottom core part	Assembled model
SHC_CYC	Square Honeycomb	Corrugated Y-shaped Core	
CYC_SHC	Corrugated Y-shaped Core	Square Honeycomb	
SHC_CXC	Square Honeycomb	Corrugated X-shaped Core	
CXC _SHC	Corrugated X-shaped Core	Square Honeycomb	
SHC_WSC	Square Honeycomb	Woven Square Core	
WSC_SHC	Woven Square Core	Square Honeycomb	
SHC_WTC	Square Honeycomb	Woven Triangular Core	
WTC_SHC	Woven Triangular Core	Square Honeycomb	

configurations were computed as shown in Eq. (7) and (8) respectively.

Variation in peak equivalent plastic strain

$$= \left(\frac{PEEQ_{,i} - PEEQ_{SHC}}{PEEQ_{SHC}} \right) \times 100 \tag{7}$$

where $PEEQ_{,i}$ and $PEEQ_{SHC}$ are the peak equivalent plastic strain value of the proposed hybrid sandwich panels and a square honeycomb sandwich structure (SHC) respectively.

$$Variation\ in\ energy\ dissipation = \left(\frac{E_{d,,i} - E_{d,,SHC}}{E_{d,,SHC}} \right) \times 100 \tag{8}$$

where $E_{d,,i}$ and $E_{d,,SHC}$ are the viscous, artificial, plastic, and total energy dissipations of the proposed hybrid sandwich panels and a square honeycomb sandwich structure (SHC) respectively.
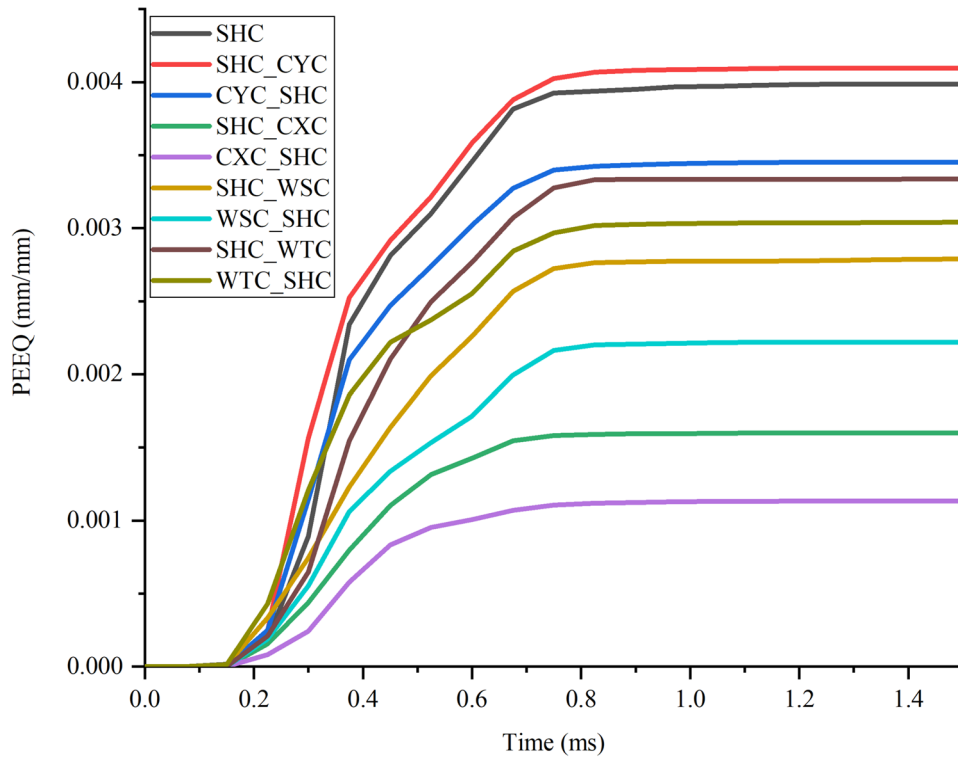
Fig. 7 Equivalent plastic strain–time history plot for a 1 kg TNT explosive charge mass
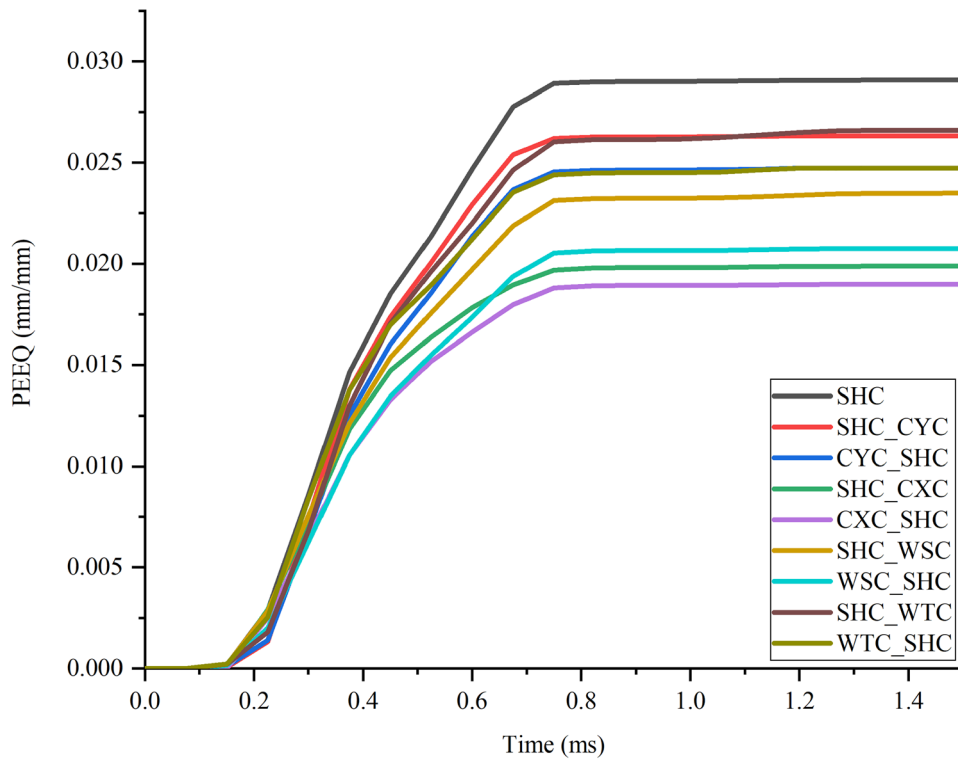
Fig. 8 Equivalent plastic strain–time history plot for a 2 kg TNT explosive charge mass
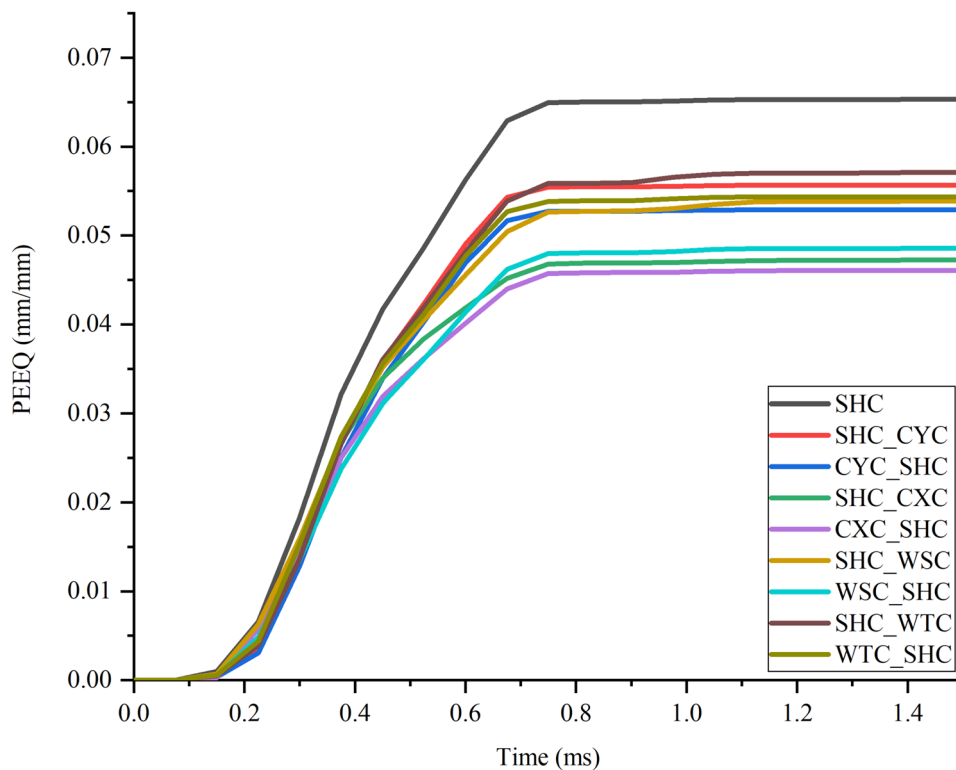
Fig. 9 Equivalent plastic strain–time history plot for a 3 kg TNT explosive charge mass
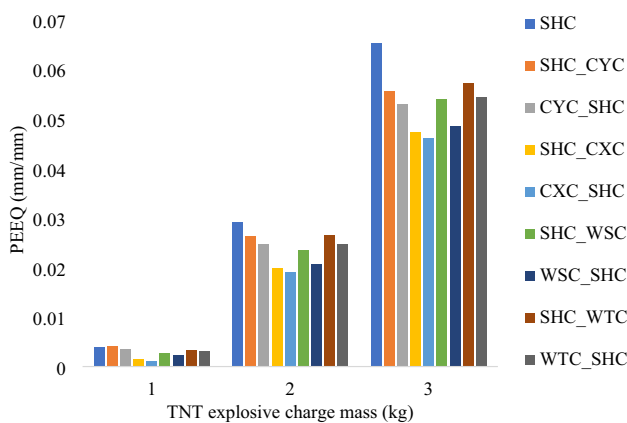
Fig. 10 Comparison of peak equivalent plastic strain values for a panels subjected to various TNT explosive charge mass

3.2 Variation in equivalent plastic strain values

Figures 7, 8 and 9 presents the equivalent plastic strain–time histories of the honeycomb and hybrid sandwich panels. To capture the damage propagation, extent of damage, and corresponding protective behavior of the structure, the equivalent plastic strain values were extracted from the back sheet of the protective system.

From the plots, it is evident that the least equivalent plastic strain values were obtained for CXC_SHC, SHC_CXC, and WSC_SHC sandwich panel structures depicting good shielding capability.

Figure 10 depicts effectiveness of use of hybrid sandwich panels when compared with the square honeycomb sandwich panel (SHC). Comparing the control honeycomb sandwich structure (SHC) with the other proposed novel hybrid sandwich structures accompanied by three TNT explosive charge masses (1 kg, 2 kg, and 3 kg), CXC_SHC, SHC_CXC, and WSC_SHC hybrid sandwich panels showed the least peak effective plastic strain values revealing better damage mitigation capability and robustness against small scaled distance blast scenarios.

As discussed in Sect. 3 (Eq. 7), for a 1 kg TNT explosive charge mass, use of CXC_SHC, SHC_CXC, and WSC_SHC hybrid sandwich panels offered a 71.6%, 59.8%, and 44.3% shield robustness capability. Likewise, for a 2 kg TNT explosive charge mass, use of CXC_SHC, SHC_CXC, and WSC_SHC hybrid sandwich panels also had a 34.7%, 31.6%, and 28.7% protective robustness capability. Moreover, for a 3 kg TNT explosive charge mass, use of CXC_SHC, SHC_CXC, and WSC_SHC hybrid sandwich panels offered a 29.5%, 27.6%, and 25.7% additional capacity to mitigate damage induced by the shock wave. The redundancy,

load path continuities, reinforced mechanisms against in-plane compression and buckling are the reasons for the low effective plastic strain values observed on CXC_SHC, SHC_CXC.

Conversely, for the three TNT explosive charge masses, SHC_CYC, CYC_SHC, and SHC_WTC hybrid sandwich panels revealed less damage mitigation capability and robustness against small scaled distance blast scenarios. For a 1 kg TNT explosive charge mass, use of SHC_CYC, CYC_SHC, and SHC_WTC hybrid sandwich panels offered a 2.8%, 13.4%, and 16.3% shield robustness capability. Likewise, for a 2 kg TNT explosive charge mass, use of SHC_CYC, CYC_SHC, and SHC_WTC hybrid sandwich panels also had a 9.5%, 15.0%, and 8.5% decrement in effective plastic strain values. Moreover, for a 3 kg TNT explosive charge mass, use of SHC_CYC, CYC_SHC, and SHC_WTC hybrid sandwich panels offered a 14.8%, 19%, and 12.6% capacity to mitigate damage induced by the shock wave (Fig. 10).

3.3 Variation in energy values

The variation in energy dissipation values of the hybrid sandwich panels was assessed by the use of a viscous, artificial, plastic, total energy-time history plots which are all extracted from the whole structure components including both the solid cover plates and inner metallic cores.

3.3.1 Viscous Dissipation Energy

Figures 11, 12 and 13 exhibits the viscous dissipation energy-time history plots of both control honeycomb and hybrid sandwich panels. In order to capture the damage mitigation capability, the viscous dissipation energy values were extracted from the sandwich structures as a whole (both metallic cellular cores and cover plates). When comparing with the control honeycomb sandwich structure (SHC) with the other proposed novel hybrid sandwich structures accompanied by three TNT explosive charge masses, it was found that the largest values of viscous dissipation energy capability were obtained from SHC_CXC, CXC_SHC, and CYC_SHC sandwich panel structures elucidating good shielding capability.

In addition to the viscous dissipation energy-time history plots, Fig. 14 presents a comprehensive plot of peak viscous dissipation energy capability and TNT explosive charge masses. For the considered TNT explosive charge masses, SHC_CXC, CXC_SHC, and CYC_SHC hybrid sandwich panels revealed larger viscous dissipation energy.

For a 1 kg and 2 kg TNT explosive charge masses, use of CXC_SHC, SHC_CXC, and CYC_SHC hybrid sandwich panels offered a 588.59%, 349.4%, 112.8%; and 215.2%, 229.8%, and 38.5% increment in viscous dissipation energy. Moreover, for a 3 kg TNT explosive charge mass, use of CXC_SHC, SHC_CXC, and CYC_SHC hybrid sandwich panels offered a
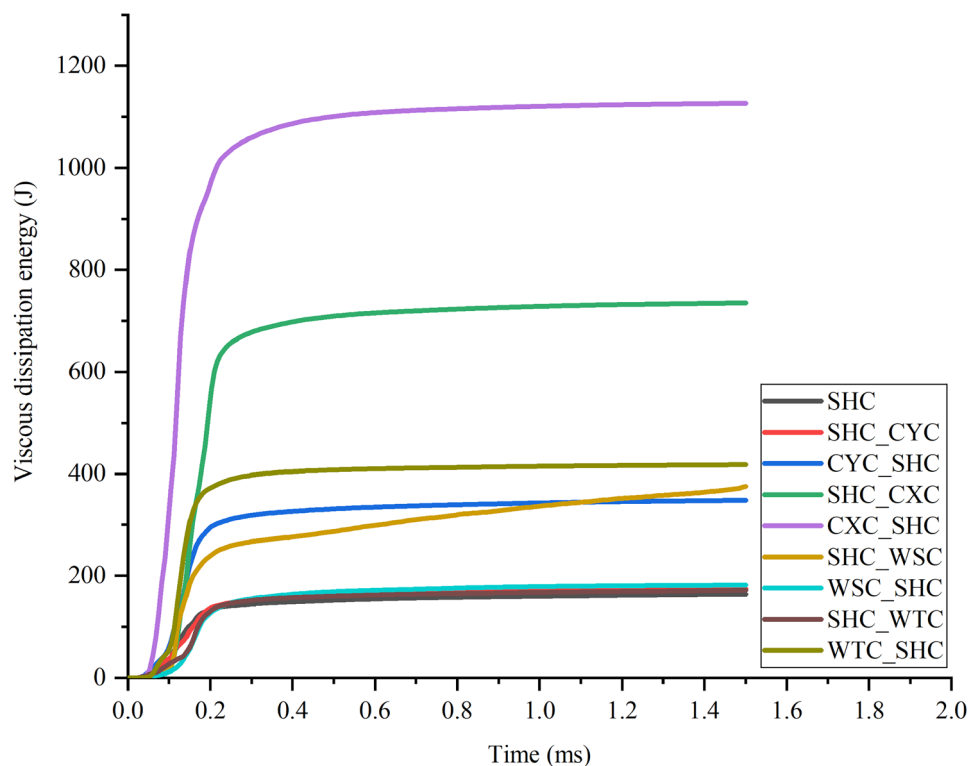

Fig. 11 Viscous dissipation energy-time history plot for a 1 kg TNT explosive charge mass
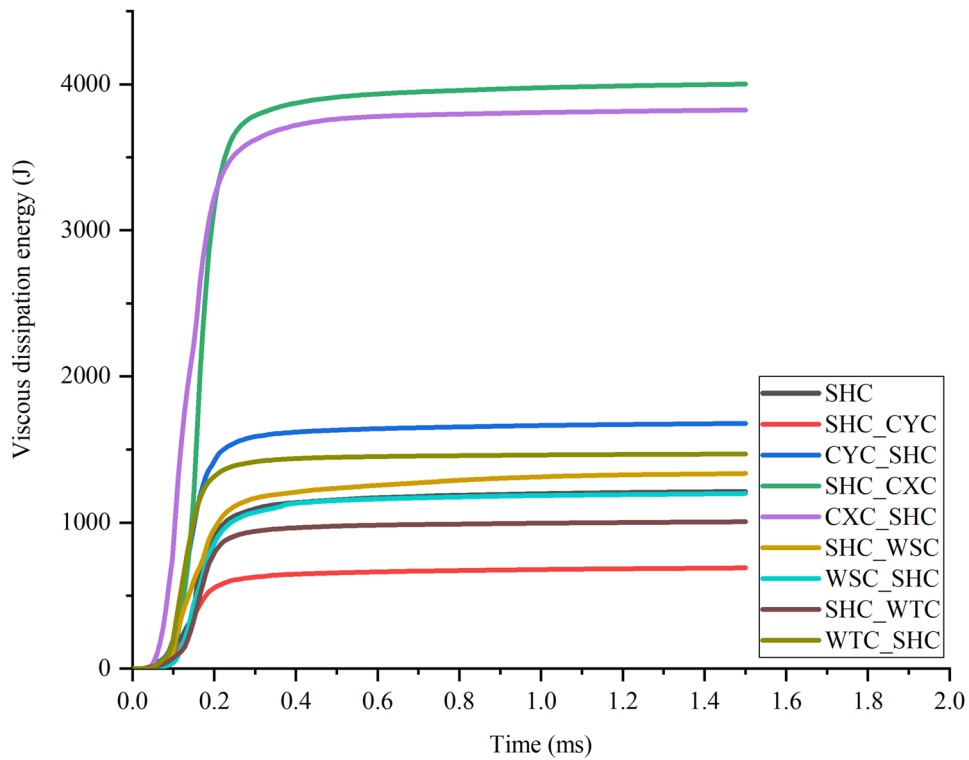
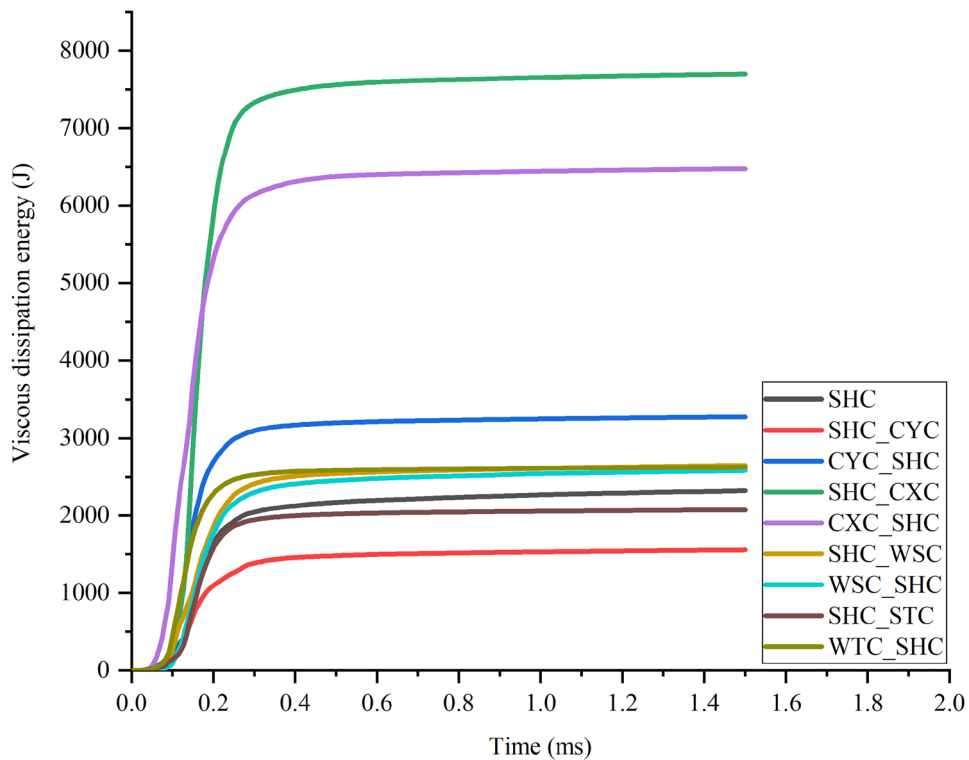**Fig. 12**   Viscous dissipation energy-time history plot for a 2 kg TNT explosive charge mass

Fig.13   Viscous dissipation energy-time history plot for a 3 kg TNT explosive charge mass
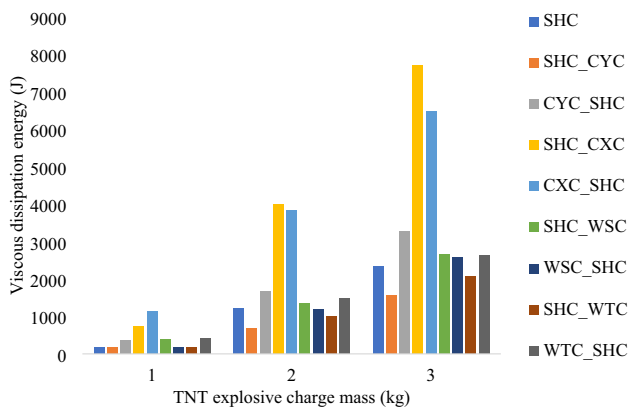
Fig. 14 Comparison of peak viscous dissipation energy values for a panels subjected to various TNT explosive charge mass

178.7%, 231.3%, and 41.1% increase in viscous dissipation energy. The redundancy, load path continuities, reinforced mechanisms against in-plane compression and buckling can be rendered as the controlling factors (reasons) for the high viscous dissipation energy values observed on CXC_SHC, SHC_CXC.

Conversely, for the considered TNT explosive charge masses, SHC_CYC, SHC_WTC, and WTC_SHC hybrid sandwich panels revealed less dissipation energy absorption capability and robustness against airblast loading scenarios. For a 1 kg TNT explosive charge mass, use of SHC_WTC, SHC_CYC, and WSC_SHC hybrid sandwich panels offered a 4.8%, 6.8%, and 11.1% increment in energy dissipation. Likewise, for a 2 kg TNT explosive charge mass, use of WSC_SHC, SHC_WSC, and WTC_SHC hybrid sandwich panels also had a 1.2%, 10.2%, and 21.2% increase in viscous dissipation energy. Moreover, for a 3 kg TNT explosive charge mass, use of SHC_WTC, WSC_SHC, and WTC_SHC hybrid sandwich panels offered a 10.7%, 11.1%, and 13% increment in viscous dissipation energy (Fig. 14).

3.3.2 Variation in Artificial Energy Values

Figures 15, 16 and 17 depicts the artificial energy-time history plots of both honeycomb and hybrid sandwich panels. From the plots, for different blast scenarios with 1 kg, 2 kg, and 3 kg TNT explosive charge masses, it is evident that the highest artificial energy value was obtained for SHC, CXC_SHC, and SHC_WSC sandwich panel structure. Whereas, for the same blast scenarios, SHC_CYC, and SHC_WSC exhibited the least artificial energy (see Figs. 15, 16 and 17).
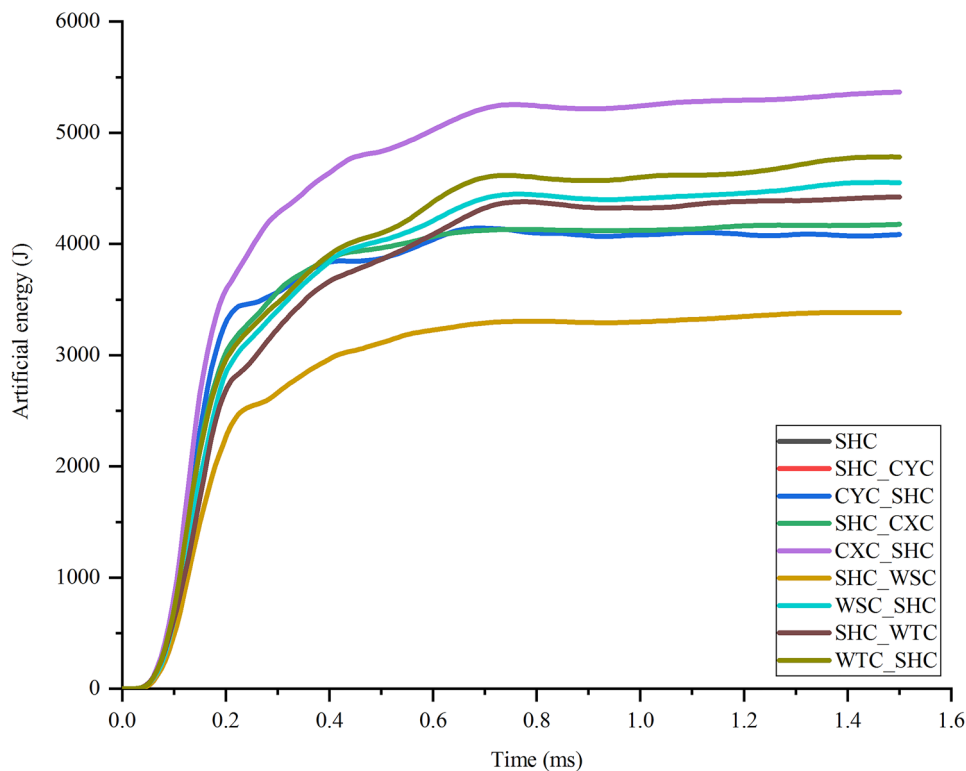
Fig. 15 Artificial energy-time history plot for a 1 kg TNT explosive charge mass
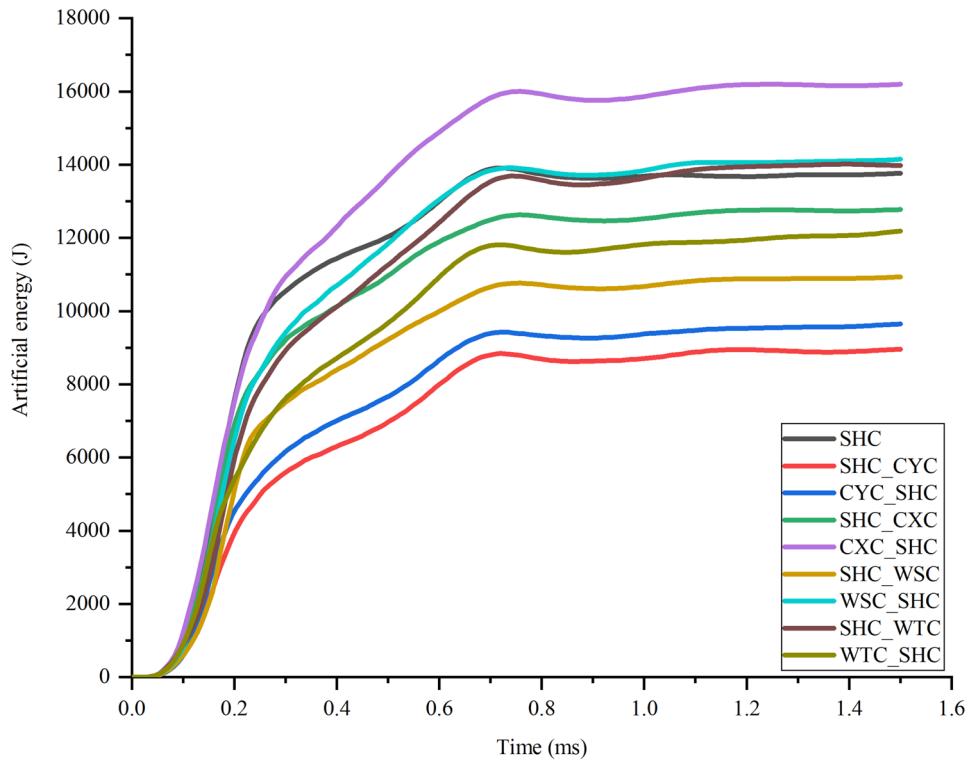
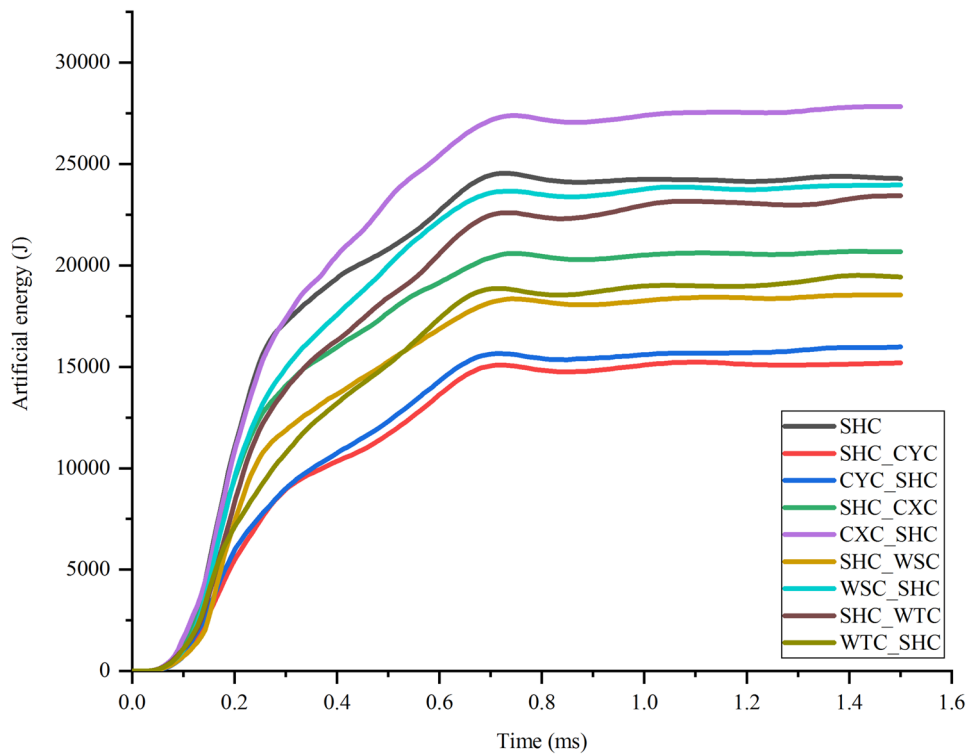**Fig. 16** Artificial energy-time history plot for a 2 kg TNT explosive charge mass

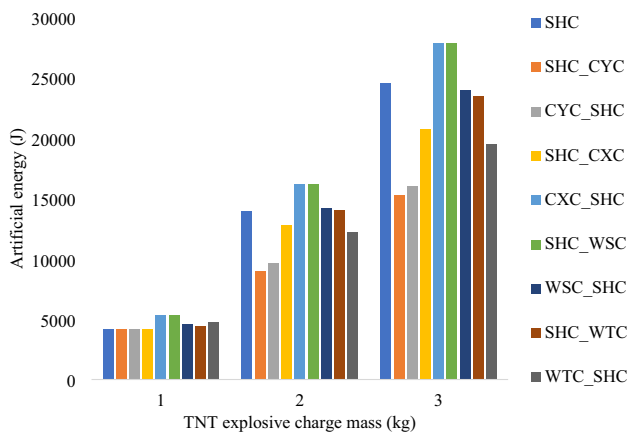**Fig. 17** Artificial energy-time history plot for a 3 kg TNT explosive charge mass

Fig. 18 Comparison of peak artificial energy values for panels subjected to various TNT explosive charge mass

Likewise, Fig. 18 presents a summary of peak artificial energy and TNT explosive charge masses. Comparing with a control core configuration (SHC), for a 1 kg TNT explosive charge masses, use of CXC_SHC, and SHC_WSC hybrid sandwich panels offered a 29.5% variation in artificial energy. Moreover, As discussed in Sect. 3 (Eq. 8), for a 2 kg and 3 kg TNT explosive charge mass, use of CXC_SHC, and SHC_WSC hybrid sandwich panels offered a 16% and

13% variation in artificial energy values respectively (see Fig. 18).

3.3.3 Variation in plastic energy

Figures 19, 20 and 21 illustrates the plastic energy-time histories of the honeycomb and hybrid sandwich panels. From the plots, for different blast scenarios with 1 kg, 2 kg, and 3 kg TNT explosive charge masses, it is shown that the trend in plastic energy variation of the considered hybrid sandwich panels was flat (see also Figs. 19, 20 and 21). Likewise, Fig. 22 presents a summary of peak plastic energy and TNT explosive charge masse values. Comparing with a control core configuration (SHC), for a 1 kg, 2 kg, and 3 kg TNT explosive charge masses, the maximum energy difference was found to be 7% exhibiting a flat trend.

Moreover, Fig. 22 exhibits a summary of peak plastic energy and TNT explosive charge masses. Comparing with a control core configuration (SHC), for a 1 kg to 3 kg TNT explosive charge masses, use of hybrid sandwich panels revealed similar and flat trend of variation.

3.4 Variation in total energy

Figures 23, 24 and 25 depict the total energy-time history plots for both honeycomb and hybrid sandwich panels.
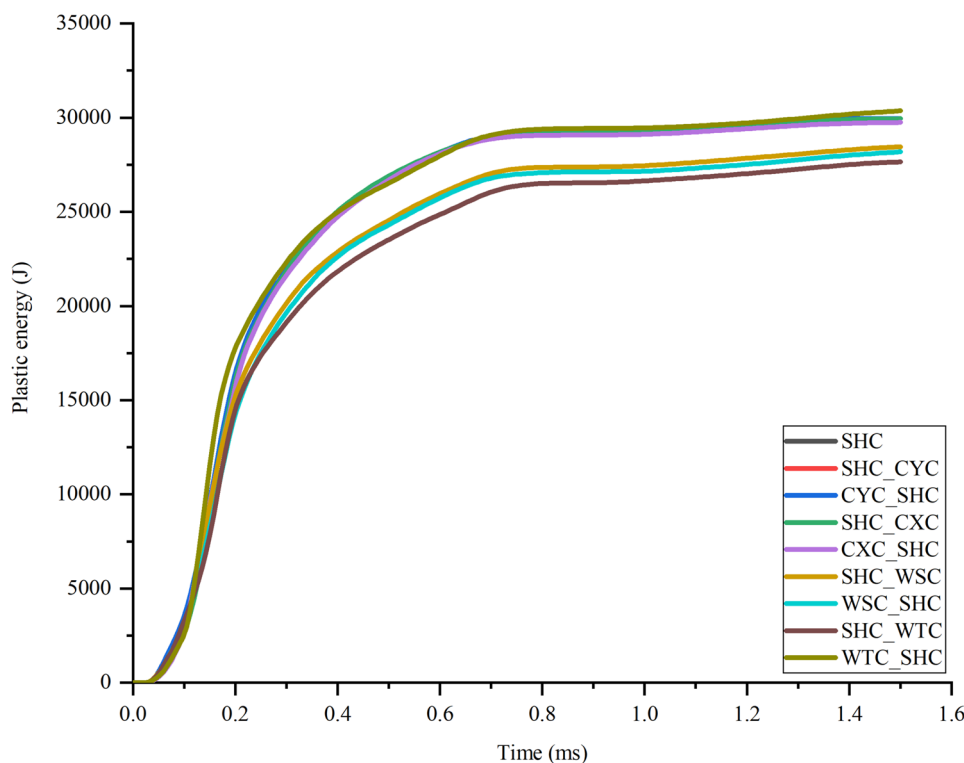

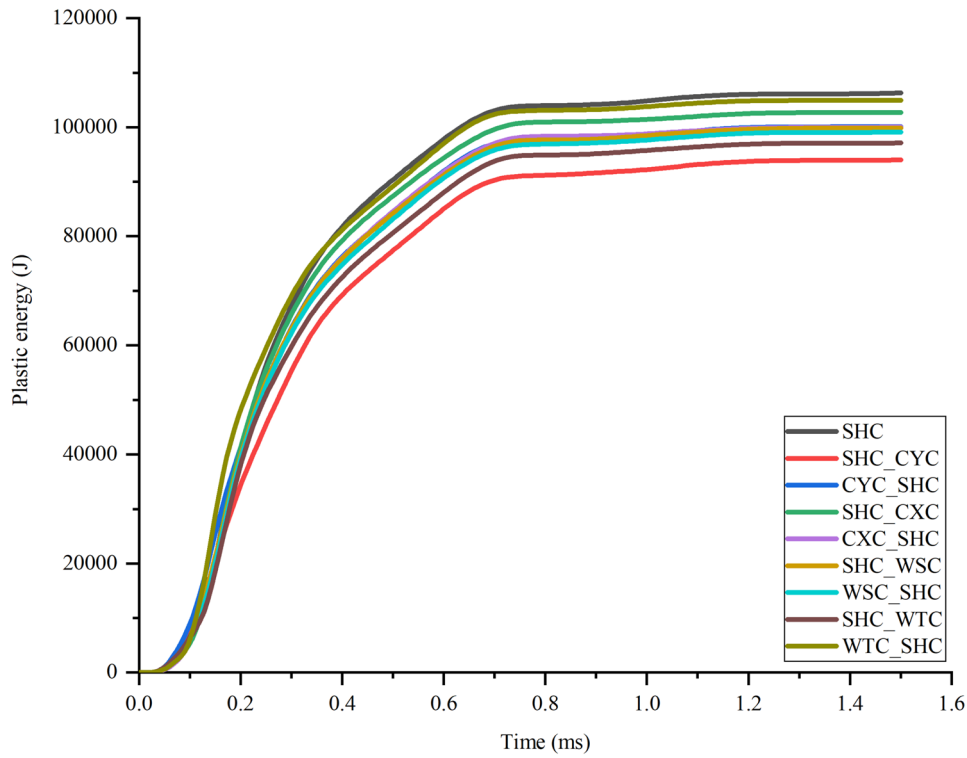**Fig. 19** Plastic energy-time history plot for a 1 kg TNT explosive charge mass

Fig. 20 Plastic energy-time history plot for a 2 kg TNT explosive charge mass
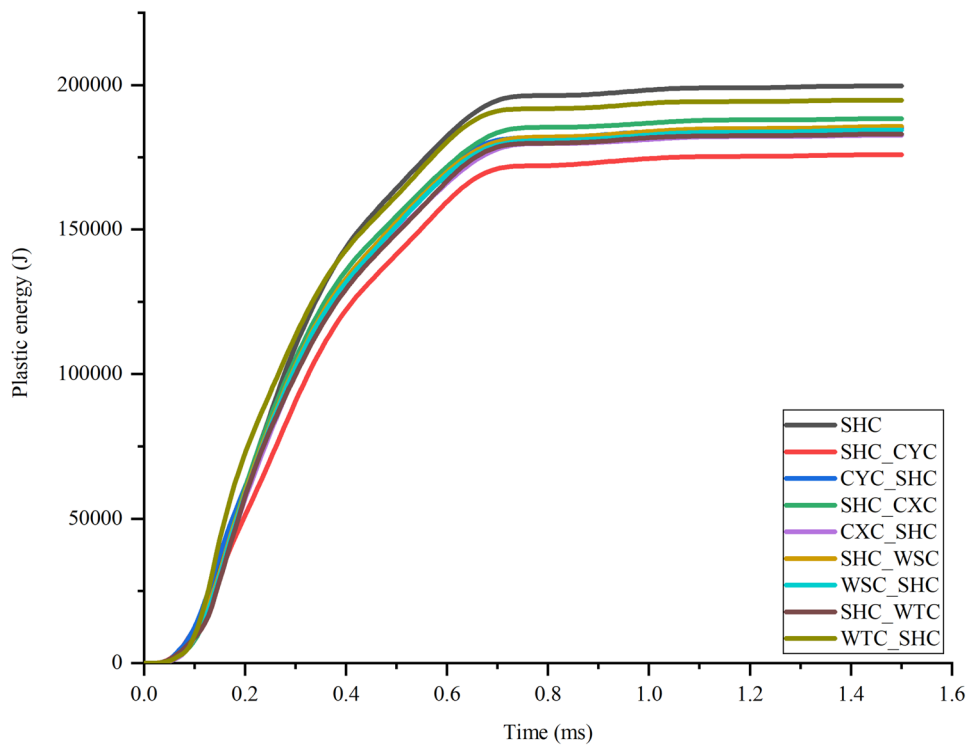

Fig. 21 Plastic energy-time history plot for a 3 kg TNT explosive charge mass
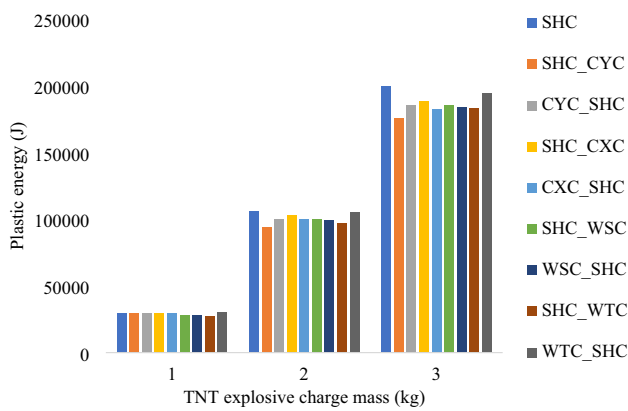
Fig. 22 Comparison of peak plastic energy values for panels subjected to various TNT explosive charge mass

The plots reveal that CYC_SHC, SHC_WTC, and SHC_WTC sandwich panel structures obtained the highest total energy values for different blast scenarios with 1 kg, 2 kg, and 3 kg TNT explosive charge masses, respectively. On the other hand, for the same blast scenarios, WSC_SHC exhibited the lowest total energy.

Furthermore, Fig. 26 provides a summary of peak total energy values for different TNT explosive charge masses. For a 1 kg TNT explosive charge, SHC, SHC_CYC, and

CYC_SHC hybrid sandwich panels exhibited maximum total energies of 30.5 J and minimum energies of 10.7 J. Similarly, for a 3 kg TNT explosive charge, the WTC_SHC hybrid sandwich panel demonstrated maximum and minimum total energies of 187.5 J and 152.5 J, respectively.

3.5 Variation in back sheet displacement

The nodal displacement–time history curves were extracted from the bottom cover plate (also known as back sheet). Figures 27, 28 and 29 illustrate the displacement–time history curves of both honeycomb and hybrid sandwich panels. From the plots, it can be observed that for different blast scenarios with a 1 kg, 2 kg, and 3 kg TNT explosive charge masses, CXC_SHC panel exhibited the least back sheet nodal displacement values. Conversely, for the blast scenarios with 2 kg and 3 kg TNT explosive charge masses, the honeycomb sandwich panel (SHC) showed the highest back sheet nodal displacement–time history values.

Additionally, Fig. 30 presents a summary of peak back sheet nodal displacement and TNT explosive charge masses. For a 1 kg and 2 kg TNT explosive charge, CXC_SHC hybrid sandwich panel showed the least recorded back sheet nodal displacement values of 25.9 mm and 34.4 mm respectively. In contrary, for 2 kg and 3 kg TNT
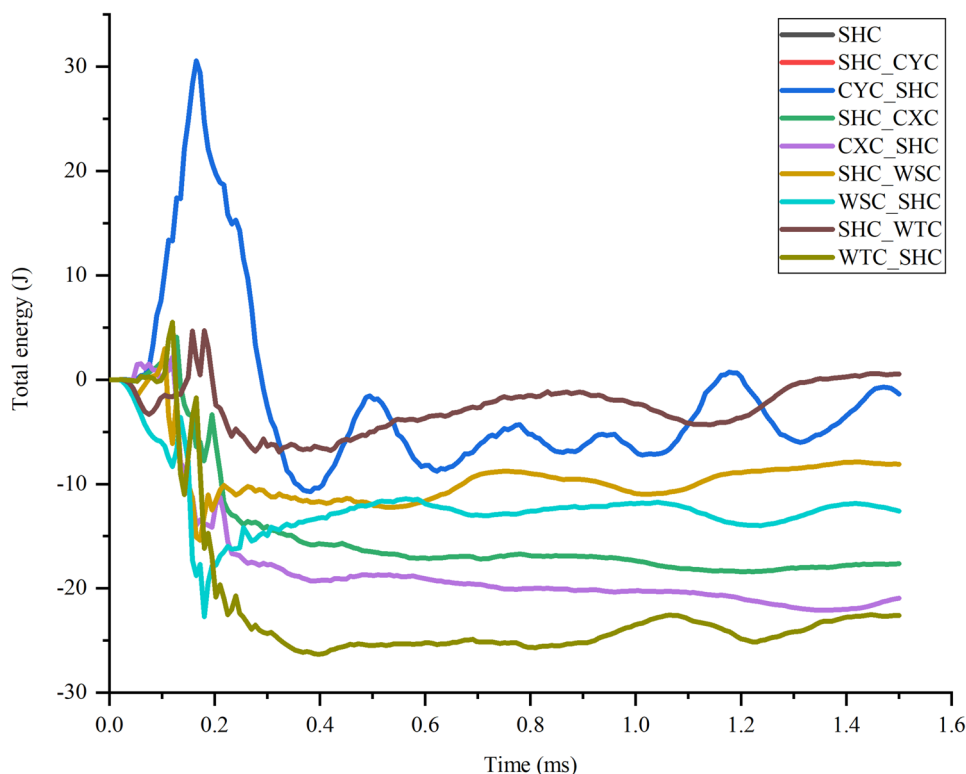

Fig. 23 Comparison of total energy versus time history curves for a hybrid sandwich panel subjected to 1 kg TNT charge mass
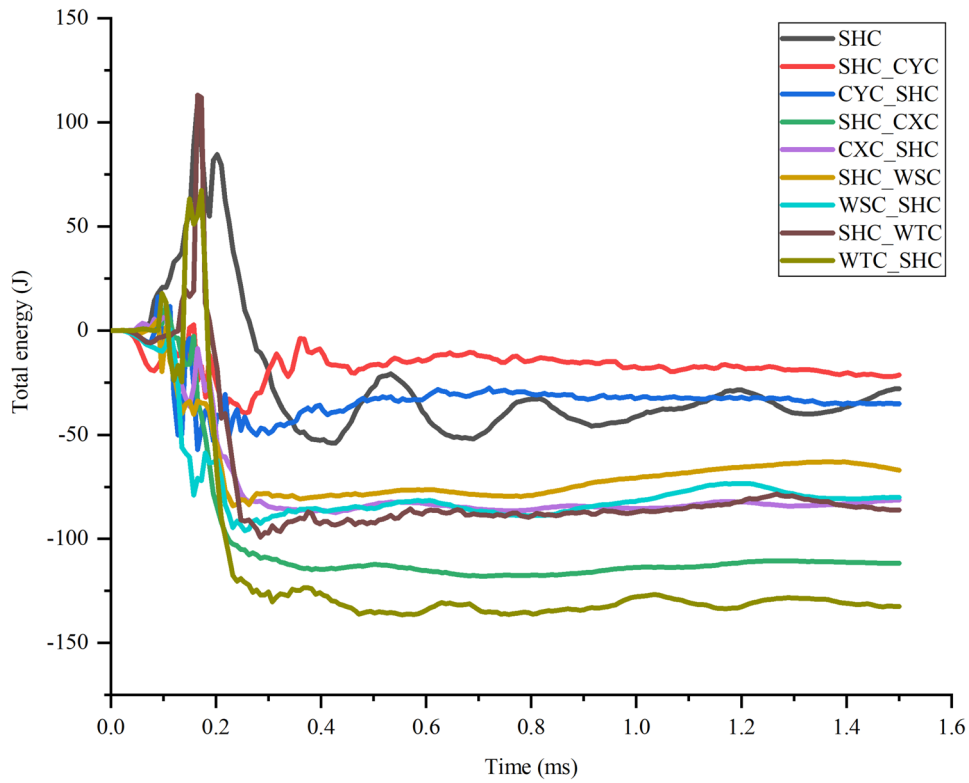
Fig. 24 Comparison of total energy versus time history curves for a hybrid sandwich panel subjected to 2 kg TNT charge mass
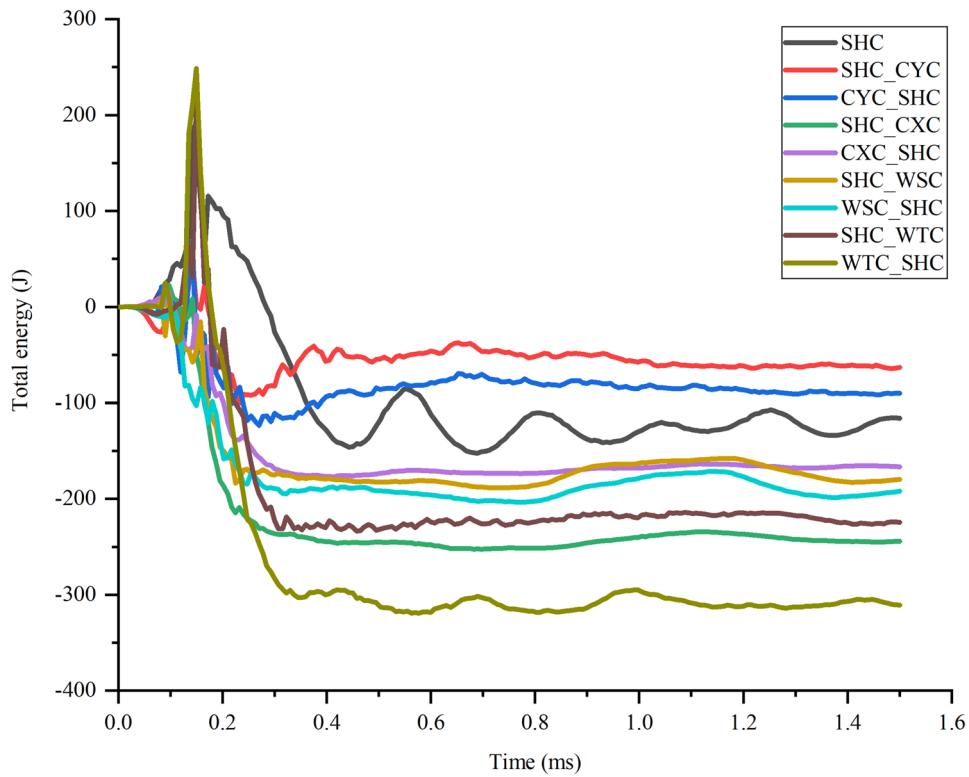

Fig. 25 Comparison of total energy versus time history curves for a hybrid sandwich panel subjected to 3 kg TNT charge mass
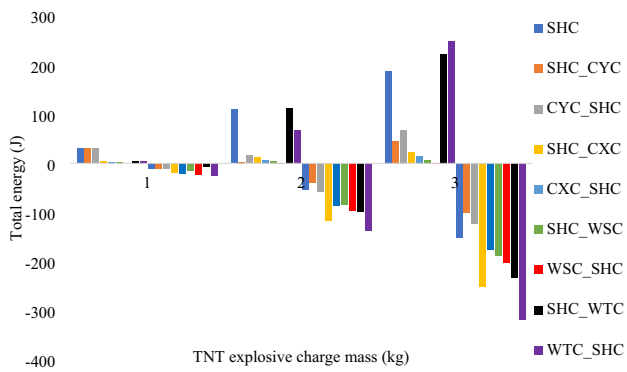
Fig. 26 Comparison of peak total energy values for panels subjected to various TNT explosive charge mass

explosive charge masses, the hybrid sandwich panel with simultaneous use of honeycomb and cross-shaped cores (CXC_SHC) sandwich panel revealed the highest nodal displacement values of 110.1 mm and 107.8 mm, respectively.

3.6 Variation in damage profile

The damage profiles of all panels were determined from the equivalent plastic strain (PEEQ) contours, taking into account various parts of the FEA models, including the bottom cover plate and interior cellular hybrid metallic cores. Figure 31, 32 and Fig. 33 display sample damage profiles of the back sheet, top cover plate, and metallic cellular cores of sandwich structures subjected to 1 kg and 3 kg TNT explosive charge masses, respectively. Near the explosive location, the sandwich structure with a honeycomb core experienced crushing and folding of cores. The square honeycomb sandwich panel showed significant damage from all blast-induced shock wave cases. Far from the explosive location, inelastic buckling was observed in the cores, with no deformation on both cover plates and cellular metallic cores where the sides are restrained (see Figs. 31a, 32a, and 33a).

Furthermore, in Figs. 31a to i and Fig. 32a to i, considering the damages induced by blast scenarios with 1 kg and 2 kg TNT explosive charge masses, the equivalent plastic strain-based damage profile extracted from the bottom and top cover plates showed that, except for the square honeycomb sandwich panel (SHC), all other eight proposed hybrid sandwich panels, especially the CXC_SHC hybrid sandwich panel, exhibited the least damage profiles. This indicates that the CXC_SHC hybrid sandwich panel possess good shielding capability against blast-induced shock waves.
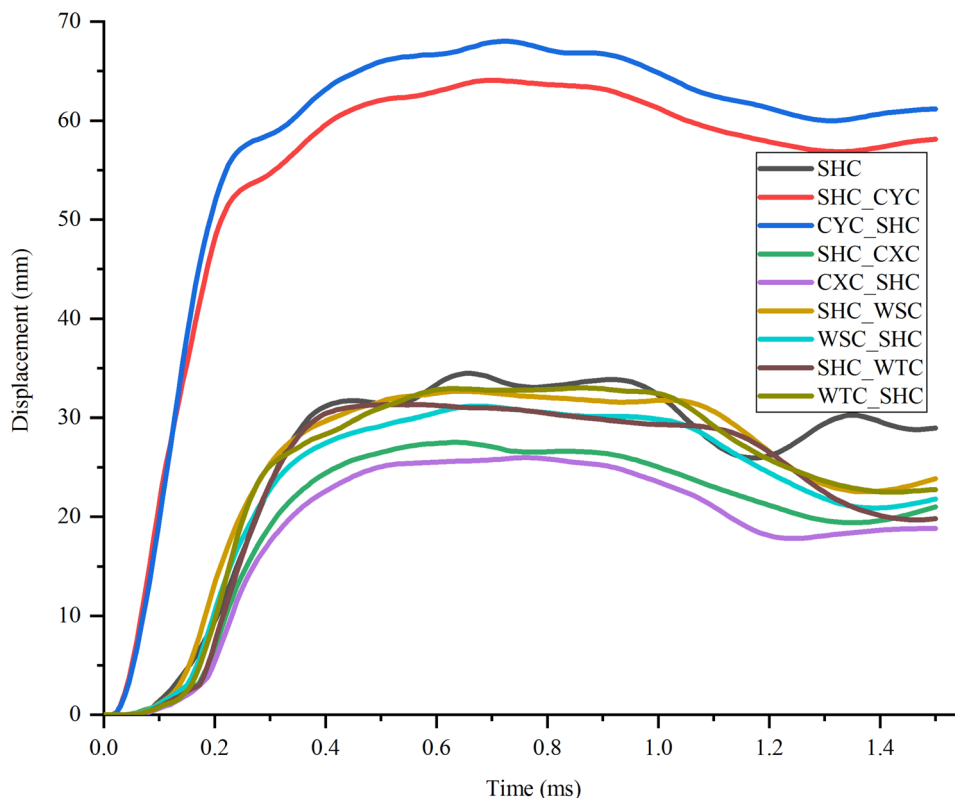

Fig. 27 Comparison of displacement–time history curves for panels subjected to 1 kg TNT explosive charge mass
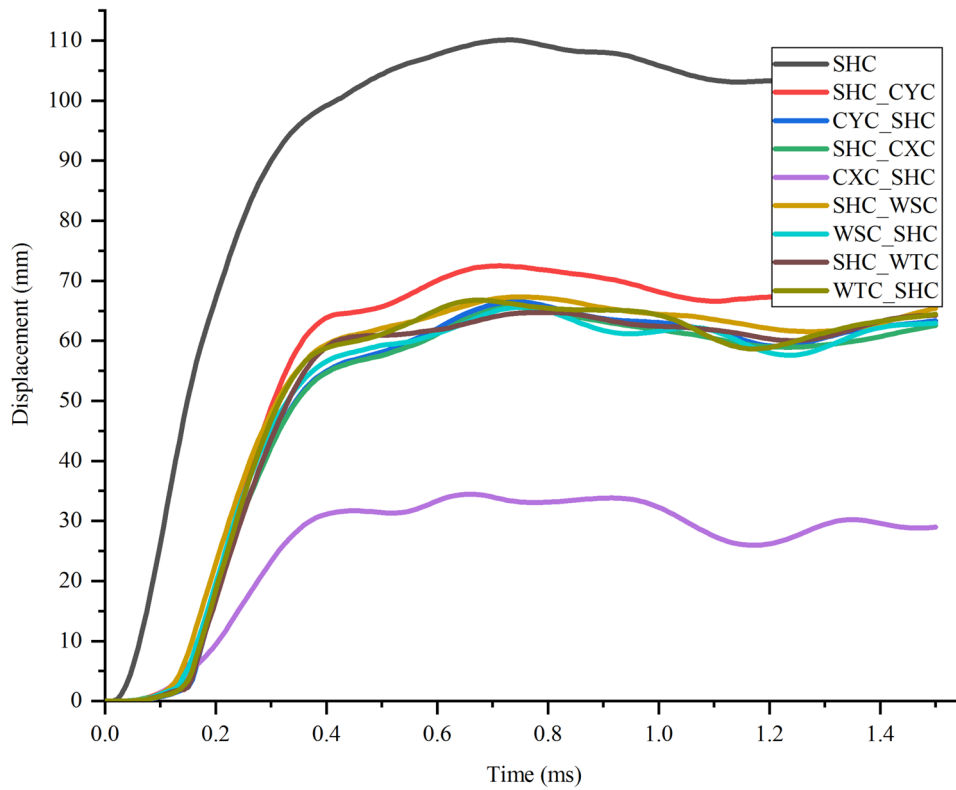
Fig. 28 Comparison of displacement–time history curves for panels subjected to 2 kg TNT explosive charge mass
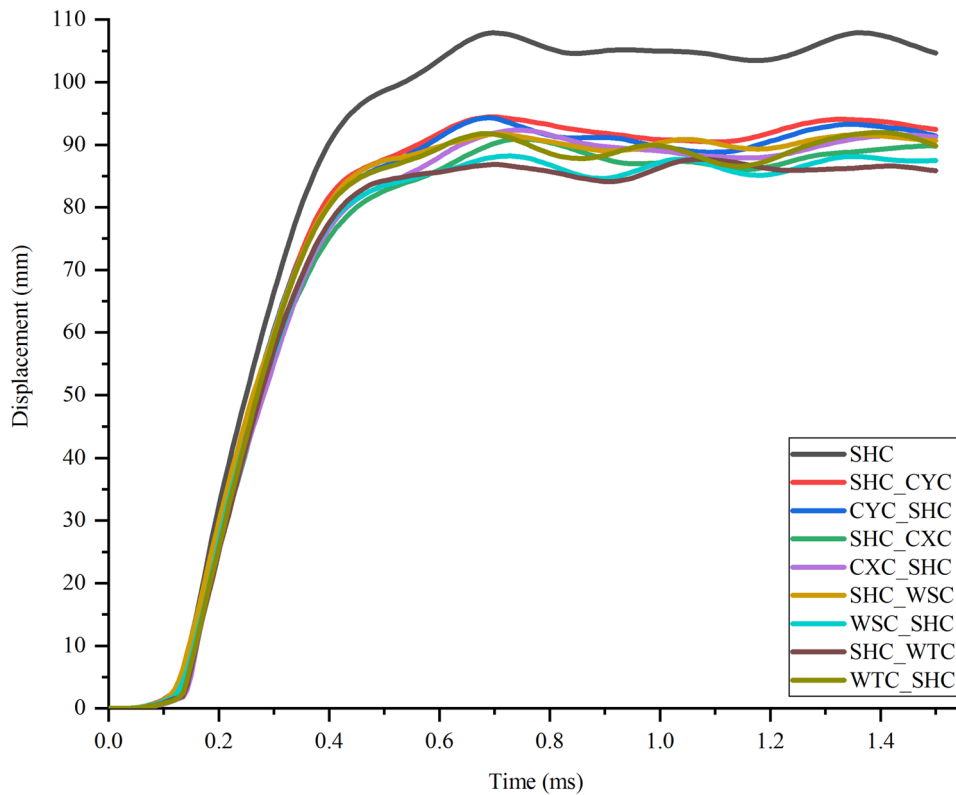

Fig. 29 Comparison of displacement–time history curves for panels subjected to 3 kg TNT explosive charge mass
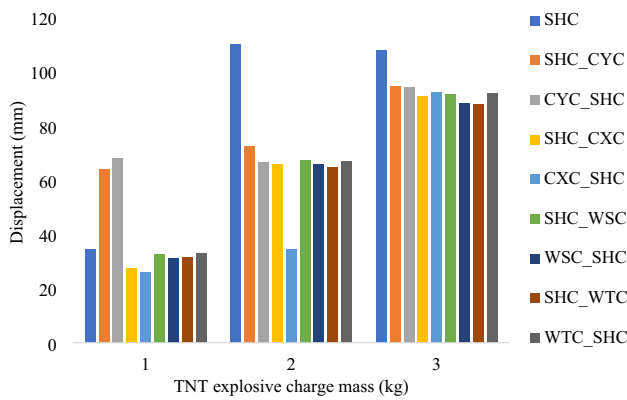
Fig. 30 Comparison of peak nodal displacement values for panels subjected to various TNT explosive charge mass

the Y-shaped corrugated cores withstand the 3 kg TNT explosive charge mass and transfer it to the honeycomb cores which were positioned at the bottom side. Because of this, the square honeycomb cores exhibited simultaneous inelastic deformations and buckling (see also Fig. 33c).

When the 3 kg TNT explosive charge mass was imposed on a hybrid sandwich structure in which the square honeycomb core was laid on the top and a corrugated X-shaped sheet was positioned at the bottom (SHC_CXC) FEA model, the square honeycomb cores which were susceptible at the first hit experienced significant crushing and inelastic bending. It is worth to note that even though the top square honeycomb cores showed damage, the X-shaped cores provide robust protection against the blast load (Fig. 33d).

Likewise, when the blast induced blast load was imposed to the reverse direction of the FEA model (CXC_SHC), the X-shaped corrugated cores withstand the 3 kg TNT explosive charge mass and revealed an outstanding performance against the blast load (see also Fig. 33e). For the same TNT explosive charge mass, a hybrid sandwich structure on which the square honeycomb core was laid on the top and a woven square core were positioned at the bottom (SHC_WSC) FEA model,
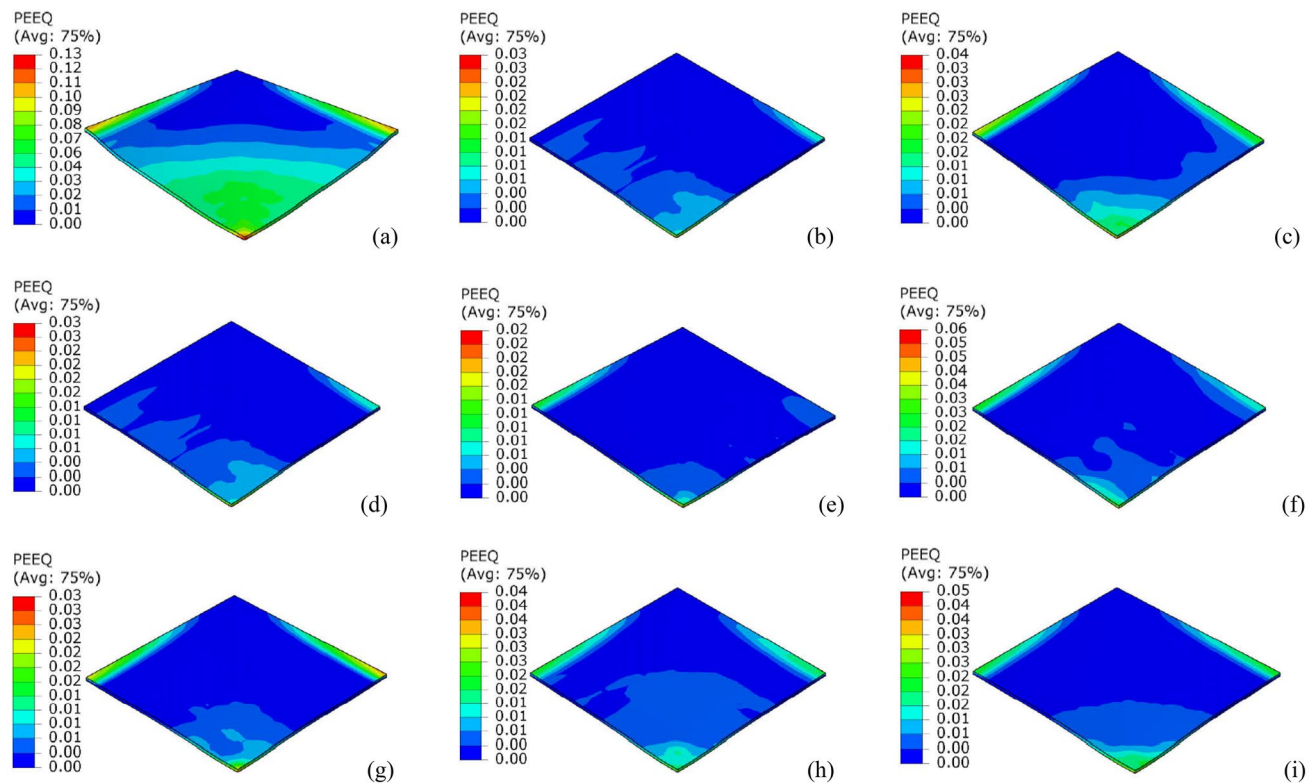
Consequently, for a blast scenario with 3 kg TNT explosive charge mass, a hybrid sandwich structure on which the square honeycomb core was laid on the top and a corrugated Y-shaped sheet was positioned at the bottom (SHC_CYC) FEA model, the square honeycomb cores which were susceptible at the first hit suffered significant tear and plastic buckling (Fig. 33b). On the other hand, when the blast induced load was imposed to the reverse direction of the FEA model (CYC_SHC),

Fig. 31 PEEQ contour plot for back sheet imposed to 1 kg TNT explosive charge mass: (**a**) SHC; (**b**) SHC_CYC; (**c**) CYC_SHC; (**d**) SHC_CXC; (**e**) CXC_SHC; (**f**) SHC_WSC; (**g**) WSC_SHC; (**h**) SHC_WTC; (**i**) WTC_SHC FEA model
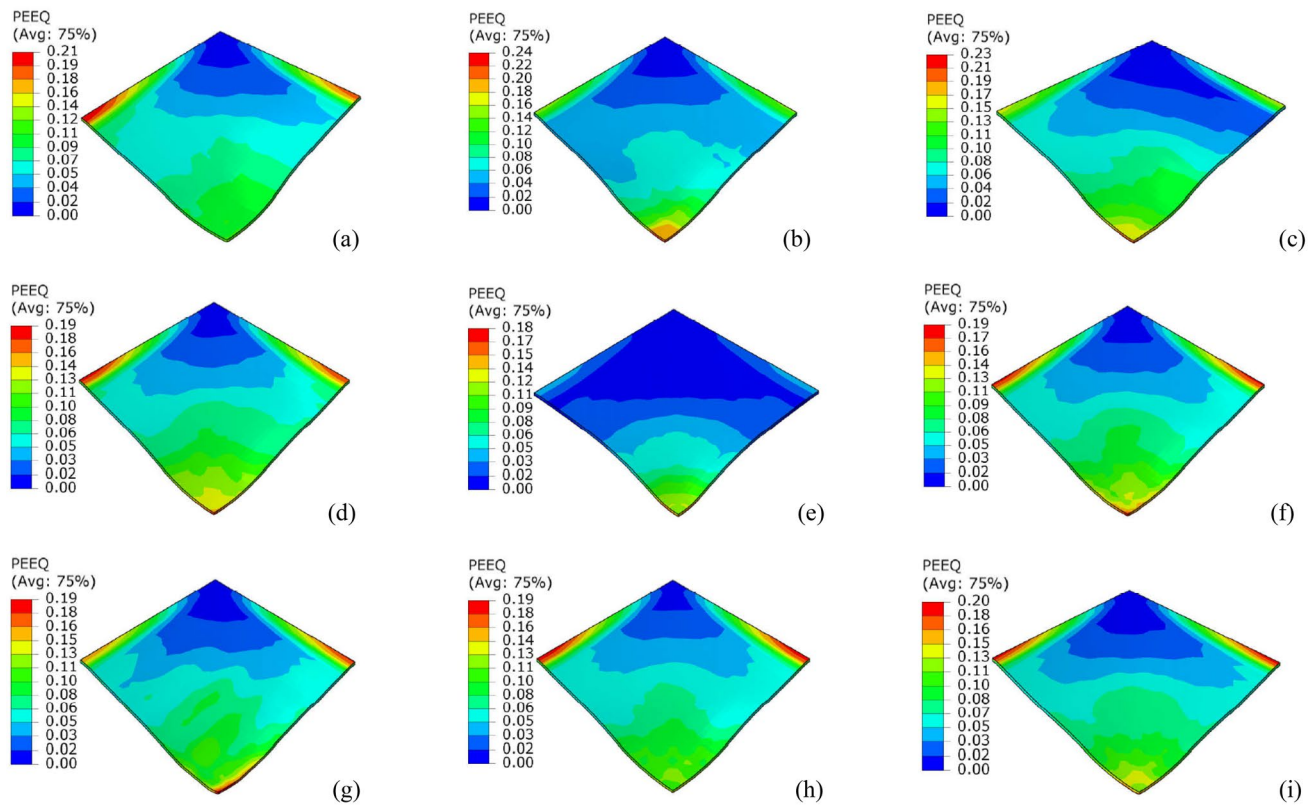
Fig. 32 PEEQ contour plot for top cover plate imposed to 2 kg TNT explosive charge mass: (**a**) SHC; (**b**) SHC_CYC; (**c**) CYC_SHC; (**d**) SHC_CXC; (**e**) CXC_SHC; (**f**) SHC_WSC; (**g**) WSC_SHC; (**h**) SHC_WTC; (**i**) WTC_SHC FEA model

the square honeycomb cores which were susceptible at the first hit experienced significant crushing and plastic buckling (Fig. 33f).

As shown in Fig. 33g, when the blast induced shock wave was imposed to the reverse direction of the FEA model (WSC_SHC), even though the horizontal component of the square shaped woven core was completely free from damage, the vertical component of the square woven core on the other hand experienced significant inelastic buckling.

The damage profile and extent of damage including folding of inner cores of the hybrid sandwich panels were captured by the FEA models. From Fig. 33h and Fig. 33i, it was shown that both the sandwich structure with triangular shaped woven core located at top and bottom experienced significant crushing and folding of cores when the explosive is located nearby. On the contrary, away from the blast source, the cores revealed inelastic buckling and at the far end sides where the sides are restrained there was no deformation (see Fig. 33h and i). The nature of the proposed structural core configuration offers the system to have better redundancy, load path continuities, reinforcing mechanisms against in-plane compression and

buckling leading to reduced damaged profiles observed in CXC_SHC, SHC_CXC configurations.

4 Conclusion

This study evaluated damage response of a metallic hybrid sandwich structures and their capability on the use of sandwich panels for protective structures against airblast. Eight metallic hybrid sandwich panels with different unexplored core configurations were investigated under the action of three various TNT explosive charge masses. The hybrid system was designed by simultaneous use of a honeycomb, corrugated sheet, and woven interlaced core configurations. The damage response of the system was evaluated by extracting the equivalent plastic strain–time history of the cover plate beyond the loaded face (bottom cover plate), damage profile for different parts of the cellular panels, back sheet nodal displacement–time history, and different energy dissipation-time history plots of the whole body including both cover plates and cores. The main conclusions are as follows:
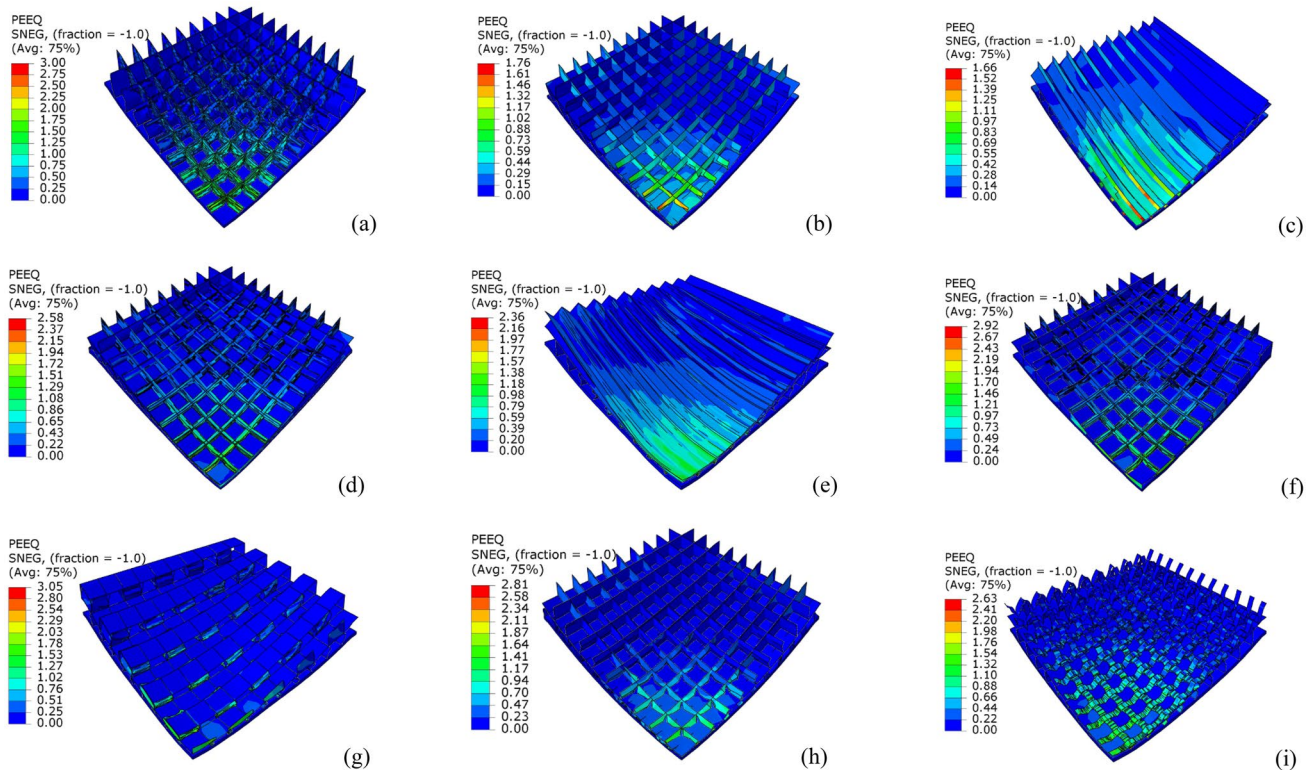
Fig. 33 PEEQ contour plot for hybrid sandwich cores imposed to 3 kg TNT explosive charge mass: (**a**) SHC; (**b**) SHC_CYC; (**c**) CYC_SHC; (**d**) SHC_CXC; (**e**) CXC_SHC; (**f**) SHC_WSC; (**g**) WSC_SHC; (**h**) SHC_WTC; (**i**) WTC_SHC FEA model

- An increase in the TNT explosive charge mass from 1 to 3 kg exhibited an increase in equivalent plastic strain, back sheet nodal displacement, and corresponding extent of damage extents.
- Comparing the hybrid sandwich panels CXC_SHC, SHC_CXC, and WSC_SHC structures with the control sandwich panel, the former revealed lower equivalent plastic strain values ranging from 25.7 to 71.6% showing an effective protective and damage mitigation capability.
- Use of SHC_CXC, and CXC_SHC metallic hybrid sandwich panels showed the highest energy dissipation values. Moreover, for all blast scenario cases with 1 kg, 2 kg, and 3 kg TNT explosive charge masses, SHC_CXC, and CXC_SHC revealed the least back sheet nodal displacement values.
- The plastic energy-time history for a blast scenario with 1–3 kg TNT explosive charge masses imposed on various hybrid sandwich panels showed a flat trend revealing insignificant variation.
- For damages induced by a blast scenario with 1 kg and 2 kg TNT explosive charge mass, the equivalent plastic strain-based damage profile extracted from the bottom and top cover plates revealed that, except for the square honeycomb sandwich panel (SHC), all other

eight proposed hybrid sandwich panels, especially the hybrid model with simultaneous use of square honeycomb and cross-shaped metallic cores, showed the least damage profiles.
- The lower effective plastic strain values and higher energy dissipation capability observed in CXC_SHC, SHC_CXC configurations were attributed due to redundancy, load path continuities, reinforcement against in-plane compression and buckling of the proposed core.

Finally, this study is limited to the investigation of metallic hybrid sandwich protective structures under airblast-induced shock waves only. Further research can expand on this work by evaluating metallic hybrid sandwich panels incorporating auxetic and biomimetic layers subjected to contact blast loading.

Declarations

Conflict of interest The authors declare that they don't have a conflict of interest.

References

1. Tarlochan F (2021) Sandwich structures for energy absorption applications: a review. Materials. https://doi.org/10.3390/ma14164731
2. Zhang L, Hebert R, Wright JT, Shukla A, Kim J-H (2014) Dynamic response of corrugated sandwich steel plates with graded cores. Int J Impact Eng. https://doi.org/10.1016/j.ijimpeng.2013.11.011,185-194
3. Ahmed S, Galal K (2019) Response of metallic sandwich panels to blast loads. J Struct Eng 1:21. https://doi.org/10.1061/(ASCE)ST.1943-541X.0002397
4. Dharmasena KP, Wadley HN, Xue Z, Hutchinson JW (2008) Mechanical response of metallic honeycomb sandwich panel structures to high-intensity dynamic loading. Int J Impact Eng. https://doi.org/10.1016/j.ijimpeng.2007.06.008
5. Luo F, Zhang S, Yang D (2020) Anti-explosion performance of composite blast wall with an Auxetic re-entrant honeycomb core for offshore platforms. J Mar Sci Eng. https://doi.org/10.3390/jmse8030182
6. Qi C, Remennikov A, Pei L-Z, Yang S, Yu Z-H, Ngo TD (2017) Impact and close-in blast response of auxetic honeycomb-cored sandwich panels: experimental tests and numerical simulations. Compos Struct. https://doi.org/10.1016/j.compstruct.2017.08.020
7. Li J, Shi S, Luo W, Wang Q (2020) Study on explosion-resistance of Biomimetic layered honeycomb structure. Adv Civ Eng. https://doi.org/10.1155/2020/5356145
8. Imbalzano G, Linforth S, Ngo TD, Lee PV, Tran P (2017) Blast resistance of auxetic and honeycomb sandwich panels: comparisons and parametric designs. Compos Struct. https://doi.org/10.1016/j.compstruct.2017.03.018
9. Al-Rifaie H, Studzinski R, Gajewski T, Malendowski M, Sumelka W, Sielicki PW (2021) A new blast absorbing sandwich panel with unconnected corrugated layers-numerical study. Energies. https://doi.org/10.3390/en14010214
10. Biagi R, Smith HB (2012) In-plane column response of metallic corrugated core sandwich panels. Int J Solids Struct. https://doi.org/10.1016/j.ijsolstr.2012.08.015,3901-3914
11. Wadley HN, Dharmasena KP, O'Masta MR, Wetzel JJ (2013) Impact response of aluminum corrugated core sandwich panels. Int J Impact Eng. https://doi.org/10.1016/j.ijimpeng.2013.06.005,114-128
12. Martinez OA, Sankar BV, Haftka RT, Bapanapalli SK (2007) Micromechanical analysis of composite corrugated-core sandwich panels for integral thermal protection systems. AIAA J. https://doi.org/10.2514/1.26779
13. Al-Rifaie H, Sumelka W (2019) The development of a new shock absorbing uniaxial graded auxetic damper (UGAD). Materials. https://doi.org/10.3390/ma12162573
14. Hou X, Deng Z, Zhang K (2016) Dynamic crushing strength analysis of auxetic honeycombs. Acta Mechan Solida Sinica. https://doi.org/10.1016/S0894-9166(16)30267-1
15. Akram S, Jaffery SI, Khan M, Fahad M, Mubashar A, Ali L (2018) Numerical and experimental investigation of Johnson-Cook material models for aluminum (AL 6061–T6) alloy using orthogonal machining approach. Adv Mechan Eng. https://doi.org/10.1177/1687814018797794
16. ABAQUS (2013) ABAQUS CAE 6.13 user's guide. RI, USA: Dassault Systèmes Simulia Corp.
17. Nahshon K, Pontin MG, Evans AG, Hutchinson JW, Zok FW (2007) Dynamic shear rupture ofsteel plates. J Mech Mater Struct 125:2049–2065. https://doi.org/10.2140/jomms.2007.2.2049